LUDWIG-MAXIMILIANS-UNIVERSITÄT
MÜNCHEN
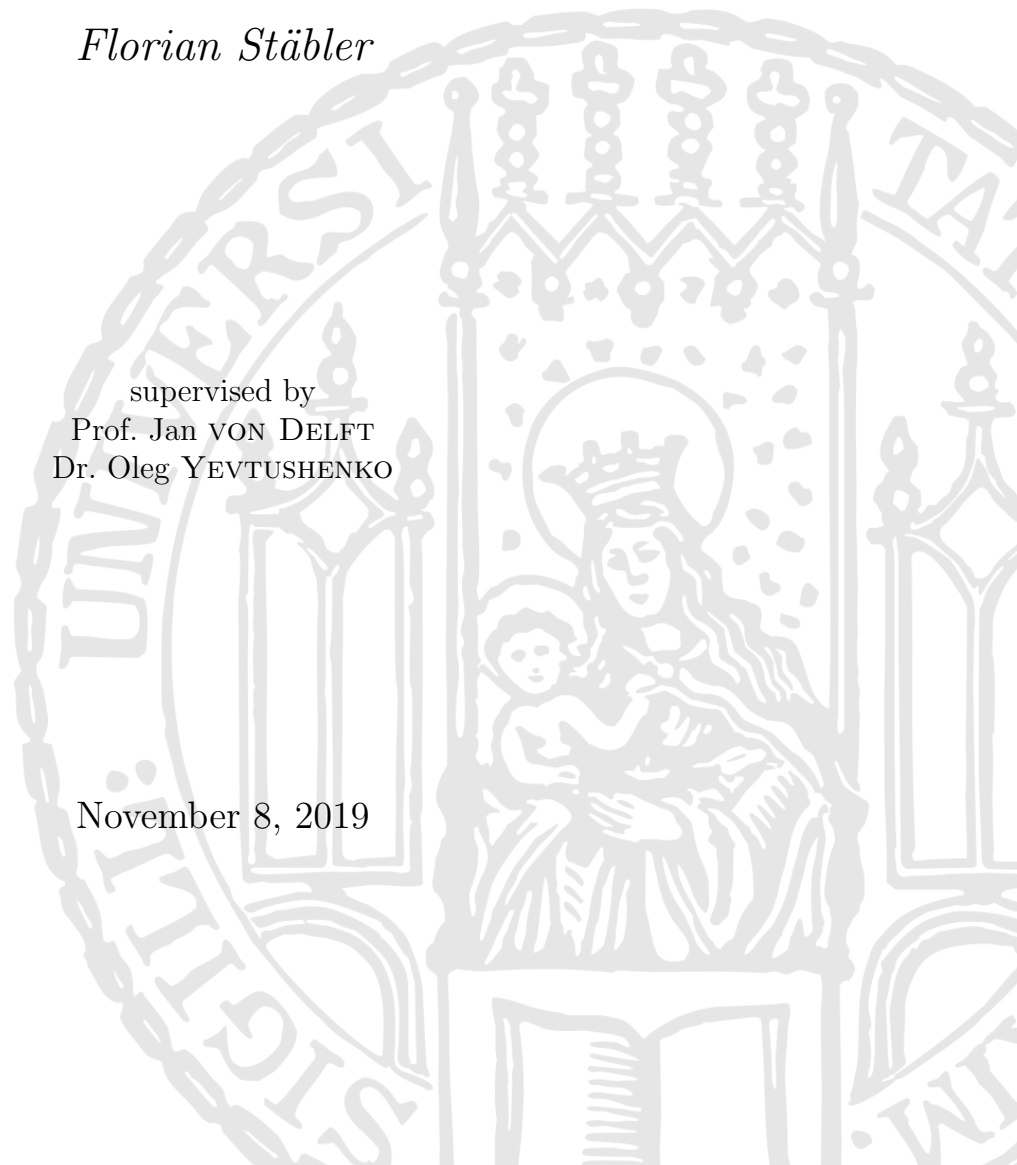
MASTER'S THESIS

# Transport properties of quasi-one dimensional magnetically doped quantum wires

*Florian Stäbler*

supervised by
Prof. Jan VON DELFT
Dr. Oleg YEVTUSHENKO
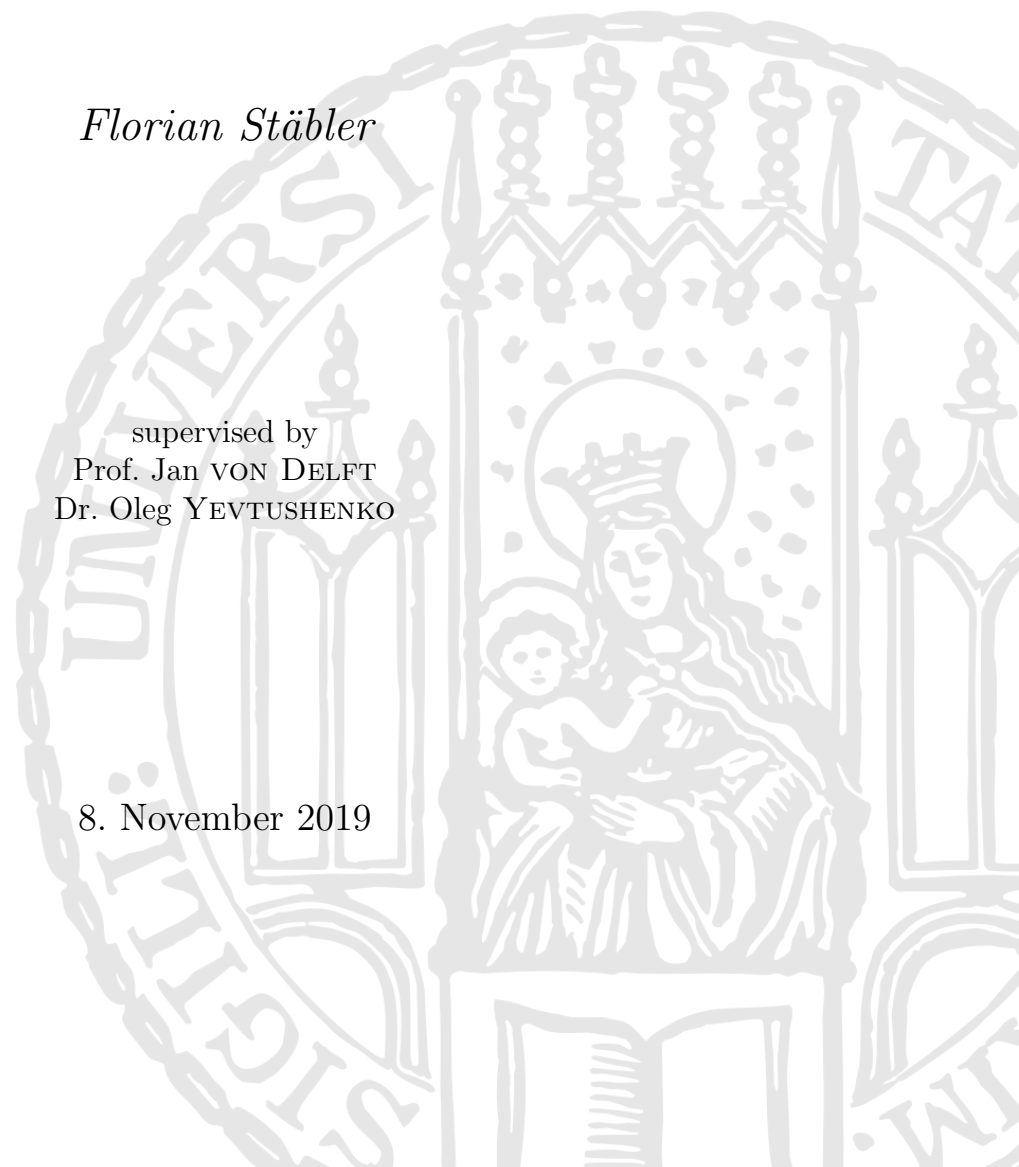
November 8, 2019

LUDWIG-MAXIMILIANS-UNIVERSITÄT
MÜNCHEN

MASTER ARBEIT

# Transporteigenschaften von quasi-eindimensionalen, magnetisch dotierten Quantendrähten

*Florian Stäbler*

supervised by
Prof. Jan VON DELFT
Dr. Oleg YEVTUSHENKO

8. November 2019

## Abstract

Magnetically doped quantum wires, theoretically modeled by a dense, one dimensional Kondo chain, are promising candidates to host protected transport carried by helical states. The hallmark of these helical state is the lock-in relation between spin and momentum, which leads to prominent properties, such as ballistic transport up to parametrically large length scales [1–4]. Helical states can also be used as a spin filter. This makes them highly promising for future nanoelectronic or spintronic devices. However, fabricating purely one dimensional systems is a highly non-trivial task. The scope of this thesis is to answer the question if strict one dimensionality is a requirement for the emergence of a helical phase. In this work, we go beyond the simplest paradigm of a one dimensional chain and analyze two Kondo chains coupled by an interchain hopping. We identified three relevant regimes, characterized by different interchain tunneling strengths and analyzed the weak and strong tunneling regime. Two weakly coupled chains exhibit a helical phase in the presence of an intrinsic Dresselhaus spin-orbit interaction. Two strongly coupled chains can support a helical phase without any spin-orbit interactions. We believe our results support the experimental detection of helical states in quasi-one dimensional systems.

# Contents

# Nomenclature

## Abbreviations

| | |
|---|---|
| 2DEG | Two dimensional electron gas |
| CHS | Chiral sublattice symmetry |
| d.o.f. | Degree of freedom |
| IQHE | Integer Quantum Hall effect |
| KC | Kondo chain |
| KI | Kondo impurity |
| PHS | Particle hole symmetry |
| QSH | Quantum Spin Hall effect |
| SOI | Spin-orbit interaction |
| TI | Topological insulator |
| TKNN | Thouless, Kohmoto, Nightingale, den Nijs |
| TRS | Time reversal symmetry |

## Symbols

| | |
|---|---|
| $c^\dagger(c)$ | Fermionic creation (annihilation) operator |
| $\mathcal{H}$ | Hamiltonian density |
| $L_n^{(\dagger)}(x)$ | Left moveing electron annihilation (creation) operator with d.o.f. $\mathbf{n}$ |
| $\mathcal{L}$ | Lagrangian density |
| $\mathbf{S}_j$ | Impurity spin of magnitude $s$ at position $j$ |
| $\sigma_{0,x,y,z}$ | $\begin{pmatrix} 1 & 0 \\ 0 & 1 \end{pmatrix}, \begin{pmatrix} 0 & 1 \\ 1 & 0 \end{pmatrix}, \begin{pmatrix} 0 & -i \\ i & 0 \end{pmatrix}, \begin{pmatrix} 1 & 0 \\ 0 & -1 \end{pmatrix}$    in spin space |
| $\tau_{0,x,y,z}$ | $\begin{pmatrix} 1 & 0 \\ 0 & 1 \end{pmatrix}, \begin{pmatrix} 0 & 1 \\ 1 & 0 \end{pmatrix}, \begin{pmatrix} 0 & -i \\ i & 0 \end{pmatrix}, \begin{pmatrix} 1 & 0 \\ 0 & -1 \end{pmatrix}$    in wire space |

| | |
|---|---|
| $R_n^{(\dagger)}(x)$ | Right moveing electron annihilation (creation) operator with d.o.f. $\mathbf{n}$ |
| $\xi_0$ | Lattice constant |
| $D$ | Band width |
| $J$ | Kondo interaction coupling strength |
| $t, t_\perp$ | Tight-binding hopping strength in longitudinal and transverse direction |

# 1

## Chapter 1

# Introduction on helical states

In this chapter we review some of the physical mechanisms which can lead to the formation of helical states and discuss basic properties of these states and their experimental manifestation. Helical states are characterized by a lock-in relation between spin and momentum. For one dimensional systems, helicity $h$ is defined as

$$h = \text{sign}\,(p) \cdot \text{sign}\,(\sigma),\qquad(1.1)$$

where sign($p$) denotes the sign of the momentum and sign($\sigma$) the sign of the spin.

## 1.1. Topolgical insulators

In mathematics, topology defines equivalence classes of shapes, which can smoothly be transformed into one another, without creating holes, gluing or cutting in the process. In condensed matter physics, one defines equivalence classes of different physical systems, which can be transformed into another, without breaking the underlying symmetries. Physical states which belong to the same topological class can be characterized by a topological invariant. Altland and Zirnbauer introduced a characterization of topological invariants depending on which symmetries are present in the system, see table 1.1 [5,6].

In 1980, von Klitzing discovered the Integer Quantum Hall Effect (IQHE) [7]. Applying an electric field along a two dimensional electron gas (2DEG) in a strong, perpendicular magnetic field at very low temperatures leads to a Hall current with a quantized transverse conductivity, see Fig. 1.1a, and quantized chiral edge states. In Table 1.1 the IQH state corresponds to class A and d = 2 of the Altland-Zirnbauer classification. The IQH state is thus characterized by a $\mathbb{Z}$ topological invariant termed the Chern number or TKNN invariant after Thouless, Kohmoto, Nightingale, and den Nijs [8]. Under the assumption of periodic boundary conditions in x and y directions of the sample, one finds

$$n = \sum_{\substack{\text{occupied}\\ \text{bands}}} \frac{i}{2\pi} \int d^2\mathbf{k} \left( \left\langle \frac{\partial u}{\partial k_x} \Big| \frac{\partial u}{\partial k_y} \right\rangle - \left\langle \frac{\partial u}{\partial k_y} \Big| \frac{\partial u}{\partial k_x} \right\rangle \right),\qquad(1.2)$$

|     | TRS | PHS | CS | d=1 | d=2 | d=3 |
| --- | --- | --- | --- | --- | --- | --- |
| A   | 0   | 0   | 0  | -   | $\mathbb{Z}$ | -   |
| AI  | +1  | 0   | 0  | -   | -   | -   |
| AII | -1  | 0   | 0  | -   | $\mathbb{Z}_2$ | $\mathbb{Z}_2$ |
| AIII | 0  | 0   | 1  | $\mathbb{Z}$ | -   | $\mathbb{Z}$ |
| BDI | +1  | +1  | 1  | $\mathbb{Z}$ | -   | -   |
| CII | -1  | -1  | 1  | $\mathbb{Z}$ | -   | $\mathbb{Z}_2$ |
| D   | 0   | +1  | 0  | $\mathbb{Z}_2$ | $\mathbb{Z}$ | -   |
| C   | 0   | -1  | 0  | -   | $\mathbb{Z}$ | -   |
| DIII | -1 | +1  | 1  | $\mathbb{Z}_2$ | $\mathbb{Z}_2$ | $\mathbb{Z}$ |
| CI  | +1  | -1  | 1  | -   | -   | $\mathbb{Z}$ |

Table 1.1: Topological invariants can be characterized by time reversal symmetry (TRS), particle hole symmetry (PHS) and a chiral sublattice symmetry (CS). Depending on the dimensionality of the system one can find either a $\mathbb{Z}$, $\mathbb{Z}_2$ or no topological invariant.

The TKNN invariant depends on the Berry curvature defined using periodic Bloch wave functions $u$ and always evaluates to an integer number.

The necessity of an integer topological invariant, is inevitable to understand the perfect quantization of the transverse conductivity. A gedankenexperiment proposed by Laughlin in 1981 can help to understand the nature of the quantization [9]. If one assumes, that the quantization is insensitive to changes in the geometry of the sample, one can consider an equivalent problem, replacing the Hall bar with a disk pierced by a magnetic flux, see Fig. 1.1b.

According to Faraday's law, increasing the flux from $\Phi = 0$ to $\Phi = \frac{h}{e}$ in an adiabatically slow time $T \gg \omega_c = \frac{eB}{m}$, leads to an induced voltage along the ring given by $U_{ind} = -\frac{d\Phi}{dt} = -\frac{\Phi_0}{T}$. If one assumes, that n electrons move through the sample in the time $T$, then the radial transverse current is given by $I_r = -\frac{Ne}{T}$, leading to a Hall resistivity given by

$$\rho_{xy} = \frac{U_{ind}}{I_r} = \frac{1}{n}\frac{h}{e^2}, \quad N = 1, 2, \ldots, \tag{1.3}$$

which precisely fits the experiment. However from Laughlin's argument it is not immediately clear why the charge $\Delta Q = ne$ transported in one adiabatic pumping cycle is an integer number. TKNN could show in 1982, that the quantity of transported charge in the Laughlin pump can be related to the Chern number in Eq. (1.2) and thus is not susceptible to smooth changes of the parameters of the system, such as the system geometry or small changes of the external magnetic field.

The existence of gapless chiral edge states can be understood in terms of a change of the TKNN invariant $n$ at the interface of the IQH sample ($n \neq 0$) and a trivial insulator, such as the vacuum ($n = 0$). If one slowly interpolates the gap between the QH state and the vacuum as a function of the distance, somewhere along the
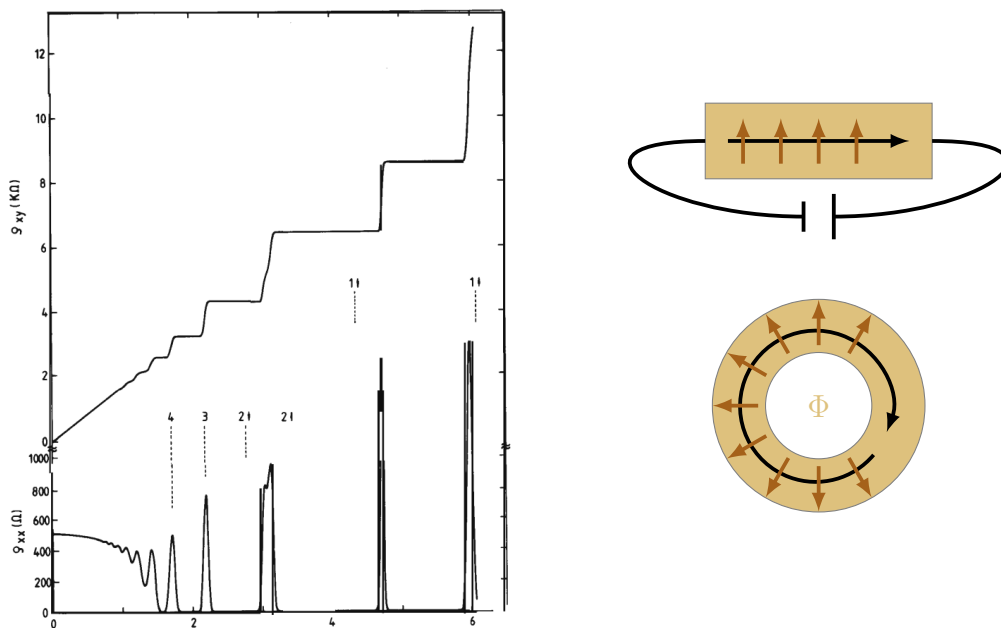
(a) Original experimental data from [7]. The upper panel shows the quantized transverse Hall conductance.

(b) Schematic depiction of Laughlin's gedankenexperiment. A hall bar can be replaced by a flux pierced disk.

interface the energy gap has to vanish, because this is the only possibility for the TKNN invariant to change. The existence of low energy gapless states near the edge is therefore guaranteed, whenever the topological invariant changes. Semiclassically, electrons near the edge of the sample perform a cyclotron motion and "bounce" of the edge of the sample leading to a chiral hopping motion. The chirality protects the transport in the sample, because single particle backscattering is not possible, if the chiral fermions on the opposing edge are spatially separated and tunneling is impossible.

The strong magnetic field in the IQH setup breaks time reversal symmetry (TRS). Haldane suggested a possibility to realize a QHE, where the net magnetic flux in the system is zero on average [10]. This lead to new ideas realizing systems, without the use of TRS breaking magnetic fields but for example spin-orbit interaction. One of the first predictions leading to a time reversal invariant system was made by Kane and Mele [11, 12] and Bernevig and Zhang [13], who showed that a two dimensional system, such as Graphene, can exhibit a quantized spin-Hall conductance and a vanishing charge-Hall conductance, while respecting TRS. The spin-Hall current is carried by helical edge states, which possess the aforementioned lock-in relation between electron spin and momentum. These systems are called Quantum Spin Hall insulators or synonymously 2D topological insulators. The QSH state consist of two copies of a QH insulator, where different spin species move with different chirality along the edge of the sample, see Fig.1.2a.

Bernevig, Zhang and Hughes proposed HgTe/CdTe quantum wells as a potential candidate to host QSH states, where it was observed by Koenig et al. in 2007 [14].
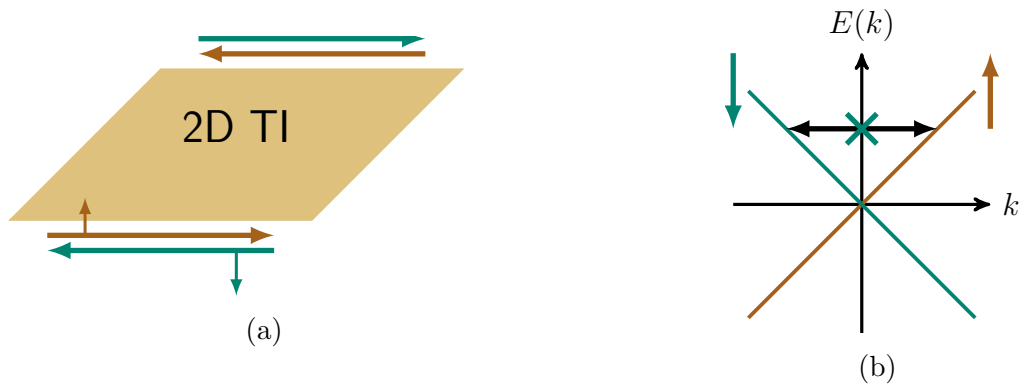
Figure 1.2: (a) Schematic helical edge state of a 2D TI. (b) Backscattering processes are not possible for U(1) spin conserving backscattering processes in 2D TI

HgTe/CdTe quantum wells show a transition to a topologically non-trivial inverted band structure above a critical width of the well, leading to helical edge states. Experimentally, this is accompanied by a drop of the conductance by a factor of two, since only helical transport is allowed at the edge. This removal of the spin degeneracy could be measured in the experiment. Another signature of helical edge states is found by applying a magnetic field, which destroys the QSH state [15].

In the Altland-Zirnbauer classification the QSH state lies in class AII and has a $\mathbb{Z}_2$ invariant, so we can have a topologically trivial state or a state with helicity $h = \pm 1$. The consequence of this is a ballistic spin current along the edge of the sample, which can serve as a basis for interesting applications such as spin filters and other spintronic applications. These helical properties of the QSH states have important properties, because backscattering on spinless impurities is forbidden, since, similar to the QH state, the counter propagating mode is on the opposite edge of the sample and thus does not participate in scattering processes.

## 1.2. Interacting systems

### 1.2.1. Spin-orbit interaction and magnetic fields

The helical properties of quantum states are not exclusively found in topological systems. Another candidate for helical states are quantum wires in the presence of strong spin-orbit interactions. Such wires can be fabricated by cleaved edge overgrowth, where a 2DEG is cut and on the interface another layer of substrate is grown to confine the electrons to a one dimensional electron gas (1DEG) or epitaxial growth of a quasi-1D structure on a substrate. Transport measurements can confirm the helical nature of the helical states produced in these setups. In wires with spin-orbit interaction the degeneracy in the dispersion relation between spin up and down electrons is removed, see Fig.1.3b. However, if one places the chemical potential somewhere in the band, one finds, that four conducting modes will always
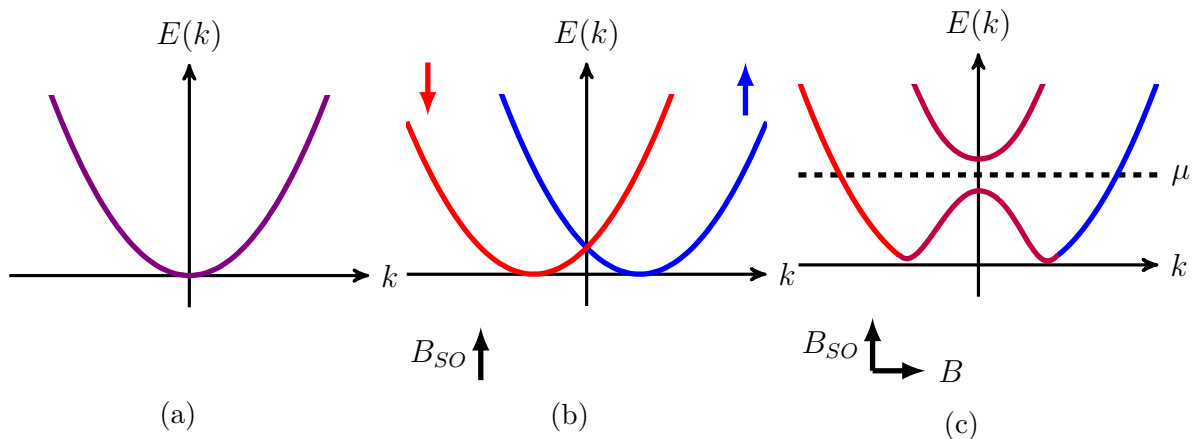
Figure 1.3: Panel (a) shows a quadratic dispersion of electrons in 1D. Panel (b) shows the effect of spin-orbit interaction. Panel (c) shows the opening of a partial gap using a B-field. Inside the gap one finds helical electrons with helicity $h = +1$, since $R_\uparrow$ and $L_\downarrow$ remain gapless.

contribute to the transport. Formally, one cannot experimentally distinguish the setup of Fig.1.3a and Fig.1.3b. Applying a magnetic field perpendicular to the direction of the spin-orbit field, mixes left and right moving spins and opens a partial gap, as shown in Fig.1.3c. The gap is partial, in the sense that only half of the fermions are gapped, depending on if they have positive or negative helicity. Assume we experimentally prepare the situation depicted in Panel (c). If the gate voltage and thus the chemical potential is tuned to lie inside of the partial gap, only half of the conducting modes participate in the transport, which can be measured as a drop of the conductance by a factor of two. If the chemical potential is tuned to lie in the upper or lower band, the conductance jumps back to its original value. This reentrant behavior in the conductance is a clear signature for helical transport in quantum wires with spin-orbit interaction. There is experimental evidence for helical states in GaAs/AlGaAs wires by Quay et al. in 2010 [16]. More recent experiments for InAs wires by Heedt et al. [17] and Kammhuber et al. [18] in 2017 could also show the reentrant behavior of the conductance.

### 1.2.2. Spin-orbit coupling in interacting quantum wires

Another possibility to realize topologically non-trivial helical states was presented by Kainaris and Carr [19]. They showed, that the spin-orbit coupling which is naturally present in a single-channel interacting quantum wire breaks the SU(2) spin symmetry and inversion symmetry. Repulsive electron-electron interaction can open a gap in the spin sector, leading to a gapped SDW-type phase which behaves similar to a topological insulator and has zero energy edge modes at the boundary of a finite system with fractional spin. It belongs to the class BDI in Table 1.1. The charge sector remains gapless and thus the wire metallic, but the bulk electron liquid shows properties similar to the edge of a Quantum Spin Hall insulator, like a quantized bulk conductance, which is robust against nonmagnetic impurities.

### 1.2.3. Nuclear magnetic field

A Luttinger liquid placed inside of a 3D lattice of localized nuclear spins can acquire a partial gap in the spectrum of the electrons. This model was theoretically studied by Loss et al. for quantum wires [20] and together with Klinovaja et al. also for carbon nanotubes [21–23].

Under the assumption, that the electrons are confined to a single transverse mode, one finds, that the nuclear spins on a cross section of the wire or CNT have identical overlap with the single transverse mode and thus identical coupling to the electrons. The exchange interaction between the nuclear spins mediated by the electrons, also called Ruderman-Kittel-Kasuya-Yoshida (RKKY) interaction, leads to a ferromagnetic alignment of nuclear spins in one plane of the wire or CNT. They effectively form large composite spins with varying magnitude for which a semiclassical one dimensional theory can be derived. Since the interaction between electrons and spins in longitudinal direction is suppressed by the number of transverse spins in the cross section one expects a separation of scales, which allows to treat the dynamics of the electrons and the nuclear spins separately. The large composite spins form a static nuclear helix, shown in Fig.1.4. This nuclear helimagnet induces an ordering of the electrons in the Luttinger liquid leading to a partial gap in the spectrum, gapping out electrons of one helicity, depending on the handedness of the nuclear helix. Electron-electron-interaction enhances the RKKY interaction and thus the formation of helical states.
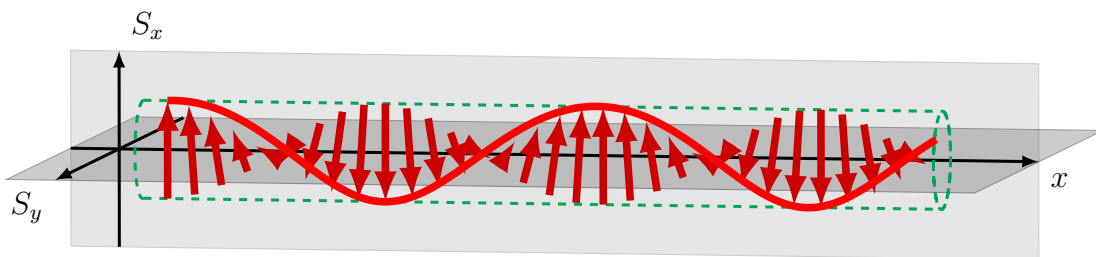


Figure 1.4: Nuclear spins are ferromagnetically aligned in a plane perpendicular to the wire and form large composite spins (red arrows). Hyperfine interaction correlates composite spins and orders them in a helix. The helical magnetic field gaps half of the fermions, leading to a helical Luttinger liquid.

There are possible experimental signatures for helical states in quantum wires in the presence of strong electron-electron interaction and in the absence of magnetic fields. Scheller et al. measured a drop in the conductance by a factor of two below a critical temperature, which hints to the formation of a helical gap in the system, which halves the number of conducting channels participating in the transport [24]. After excluding many other possibilities to obtain a reduced conductance, the influence of nuclear magnetic spins on the conductivity can be used as a possible explanation for these results.

### 1.2.4. Magnetically doped quantum wires

In this thesis, we consider magnetically doped quantum wires, another physical setup where helical transport can appear. Itinerant electrons interact with localized quantum magnetic impurities, see Fig.1.5. Possible experimental realizations of this



Figure 1.5: A 1D quantum wire doped with magnetic adatoms. Electrons and impurity can interact via their spin.

system can be GaAs/AlGaAs quantum wires or carbon nanotubes doped with magnetic atoms [25–27]. Recent observations showed, that hinges of epitaxially grown Bismuth towers present viable platforms to host one dimensional states [28]. Functionalized with magnetic atoms, they can form magnetic quantum wires.
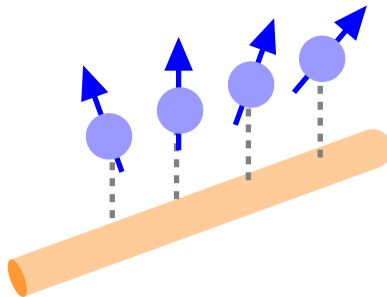
Another candidate can be found in iron based quasi-1D crystals, which have co-existing localized and delocalized electrons [29], the localized electrons playing the role of the impurities. However, a crystal structure needs to be found, where no three dimensional magnetic ordering appears. The structure of $BaFe_2Se_3$ seems to order three dimensional [30]. A more recent experimental approach uses clouds of ultra cold atoms, such as rare earth metals like Ytterbium to create a 1D system with simultaneously localized and delocalized atoms [31, 32]. The theoretical model describing this physical system is called the Kondo chain (KC), which is introduced in the next section. There is no exact solution for the Kondo chain, however, much is known from analytical and numerical studies, such as phase diagrams and ground-state properties of the KC [33–45] .

Tsvelik and Yevtushenko showed, that a KC with strong XXZ- anisotropy at in-commensurate filling in a regime dominated by indirect exchange interaction can host helical states [1]. This exchange interaction between spins forms an impurity spin helix, which spontaneously breaks the helical $\mathbb{Z}_2$ symmetry between fermions with helicity $h = 1$ and $h = -1$ and depending on the handedness of the helix, leads to helical states with either $h = 1$ or $h = -1$ in the KC. This is reflected in the fact, that the dynamical in-plane spin susceptibility $\langle S_+(j)S_-(j+1)\rangle = \langle S_x(j)S_x(j+1)\rangle - i\langle S_x(j)S_y(j+1)\rangle$ has a peak at either $2k_F$ or $-2k_F$, but not both, as one finds for the phase which hosts no helical states. The spectrum of the KC becomes gapped for fermions with a given helicity and remains gapless for the other half of the fermions.

In contrast to the system studied by Loss and Klinovaja et al. [20, 21, 23] the impurities form a single 1D chain of small, quantum mechanical spins with constant magnitude. The theoretical description by Tsvelik and Yevtushenko accounts for the quantum nature of the spin and leads to a dynamically generated spin helix in contrast to the static nuclear helix.

Schimmel et al. [4] demonstrated the robustness of the ideal charge transport of the helical modes. The transport remains ballistic even in the presence of weak random spinless disorder. Similar to the 2D TIs, single particle backscattering processes are impossible, due to the partial gap in the spectrum of the fermions. Multi particle processes are strongly suppressed in the helical phase. This protection relies on the assumption of U(1) spin conservation and holds up to parametrically large scales. The authors of Ref. [46] showed, that the spin conservation is a crucial ingredient of protected transport. Weak electron-electron interaction mixes the helical sectors, but cannot remove their protection. The qualitative picture of helical modes thus remains valid.

In the more recent work, Tsvelik and Yevtushenko showed that a strong anisotropy is not a necessary requirement for protected states in the KC. Depending on the strength of the Kondo interaction and the filling of the band, an isotropic KC can host a variety of different states [2, 3]. At special commensurate fillings one finds an insulating behavior of the Kondo chain. In the close vicinity of special commensurate fillings one finds a heavy Luttinger liquid phase, which is very sensitive to spinless disorder. At generic fillings, far from half or quarter filling, one finds a helical metal phase, where effects of disorder are again parametrically suppressed. Mermin–Wagner theorem states that no continuous symmetry can be spontaneously broken in one or two dimensional systems at finite temperatures. The breaking of the SU(2) symmetry of the Kondo interaction looses the notion of fixed spin quantization axis. This means, that the isotropic Kondo chain looses its applicability as a spin filter, since SU(2) symmetry is only locally broken and restored through slow spin fluctuations.

# 2 Chapter 2
## Physics of the 1D Kondo Chain

## 2.1. The model

In this Section, we review the physics of the KC and discuss how helical states emerge in the anisotropic 1D KC [1,4]. The Kondo chain includes itinerant electrons, interacting with localized quantum magnetic impurities. This system is described by the following Hamiltonian

$$\mathcal{H} = \overbrace{\sum_{j,\sigma} -t\left(c_{j+1}^\dagger\, c_j + h.c.\right)}^{\mathcal{H}_0} + \overbrace{\sum_{\substack{m\,\in\,M,\sigma,\sigma' \\ a\,=\,x,y,z}} J_a\, c_{m,\sigma}^\dagger\, \mathbf{S}_m^a \cdot \boldsymbol{\sigma}_a^{\sigma\sigma'}\, c_{m,\sigma'}}^{\mathcal{H}_{KI}}, \tag{2.1}$$

where $t$ is the hopping matrix element along the chain, $c_j^\dagger(c_j)$ creates (annihilates) an electron at lattice site $j$, $\mathbf{S}_j$ is the operator of a spin $s$ magnetic impurity localized at lattice site $j$, $\boldsymbol{\sigma}_a$ is a vector of Pauli matrices which acts on the spin degree of freedom and $M$ denotes a subset of all lattice sites. $J$ describes the interaction strength between itinerant electrons and the magnetic impurities.

### 2.1.1. Kondo effect vs. RKKY

The physics of the Kondo chain is governed by two competing effects. A magnetic impurity in the chain can be screened by the itinerant electrons, leading to the Kondo effect, see Fig.2.2a. At low temperatures the Kondo interaction leads to a hybridization of conduction electrons and localized impurities, opening a small hybridization band gap [47, 48].

If the chemical potential lies inside of the hybridization gap, one finds an insulating phase termed Kondo insulator, see Panel 2.1b. If one tunes the chemical potential to lie inside of the conduction band or one applies a magnetic field effectively pushing states above the chemical potential, one finds a transition from a Kondo insulator to a heavy fermion phase, see Panel 2.1c. In this phase the electron's mass becomes highly renormalized, which is reflected for example in a high electrical resistivity. If more than two impurities are present, there is also an indirect exchange interaction between localized spins, an effect, which is in strong competition with the

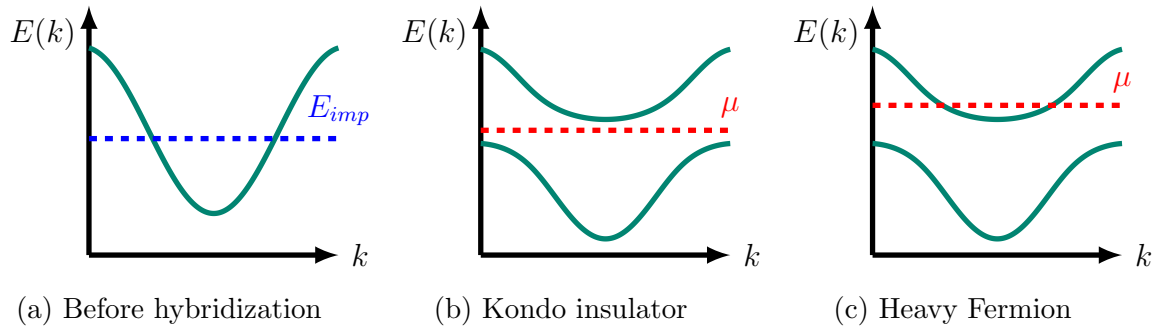(a) Before hybridization     (b) Kondo insulator     (c) Heavy Fermion

Figure 2.1: Panel (a) shows the dispersion of itinerant electrons and of the impurity before hybridization. After the hybridization a narrow band gap opens. Depending on whether the chemical potential is placed inside of the gap or in the conduction band, one finds a Kondo insulator Panel (b) or a heavy fermion phase Panel (c)

Kondo effect, see Fig.2.2b. Instead of screening individual impurities, the conduction electrons mediate an interaction between neighboring spins and correlates them.

The dominating effect can be found from Doniach's phase diagram for 1D KCs [49], which is based on the comparison of the typical energy scales of both effects, see Fig.2.2c. The red curve of Fig.2.2c shows the energy scale of the Kondo temperature $T_K \sim \exp\{-1/(\vartheta(E_F)J)\}$ for one impurity, which gives an estimate for the energy scale of the Kondo effect. The blue curve of Fig.2.2c shows the energy scale of the Ruderman-Kittel-Kasuya-Yoshida (RKKY) interaction, which can be obtained by perturbatively integrating out the itinerant electron operators in Eq. (2.1) up to second order of the coupling strength $J$. It is thus given by $T_{RKKY} \sim \vartheta(E_F)J^2$.



(a) Kondo effect     (b) Ind. ex. interaction     (c) Phase diagram
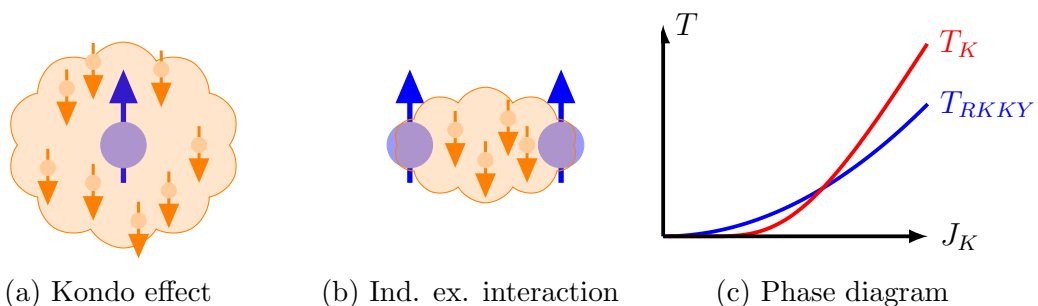
Figure 2.2: Schematic illustration of different regimes present in the the Kondo chain. In Panel (a) the Kondo effect is shown, where magnetic impurities are screened individually by the itinerant electrons. In Panel (b) the conduction electrons mediate an interaction between two spins. Panel (c) shows Doniach's phase diagram, which compares the energy scales of the Kondo effect $T_K \sim \exp\{-1/(\vartheta(E_F)J)\}$ with the RKKY interaction $T_{RKKY} \sim \vartheta(E_F)J^2$

If J is weak, there is a crossover from the Kondo regime to the regime dominated by indirect exchange interaction. The crossover can be formulated as an requirement for the denseness of the lattice we are considering. Comparing energy scales gives

$$\xi_{cr} \sim \xi_0 \left[ \frac{\vartheta(E_F) J_K^2}{T_K} \right]^{\frac{1}{2}}. \tag{2.2}$$

If the spin lattice constant is small $\xi_s \ll \xi_{cr}$, the physics is dominated by RKKY interaction. Not only the physics in KCs are mutually exclusive, but also the physical mechanisms generating them. The authors of Ref. [36] considered an interaction generated by forward scattering. This leads to a Kondo type physics. It was shown in [1–4], that a RKKY type interaction leads to a physics dominated by single particle backscattering processes. For a single impurity sitting at the origin right- and left-moving fermions R(L) have an almost interchangeable role. One can unfold the setup by a transformation of the form $R(x) = L(-x), x > 0$, such that forward and backscattering lead to similar physics. In this thesis we are considering Kondo lattices, for which this is not possible and therefore the physics of forward scattering and backscattering are mutually exclusive. For the following analysis we thus neglect forward scattering processes.

### 2.1.2. Prerequisites to find helical states in KCs

Let us summarize assumptions which were used in the previous papers [1,4] and will be used below in the current thesis:

- We consider an anisotropic model, where $J_x = J_y = J_\perp \gg J_z \to 0$

- The Kondo coupling strength is much smaller than the band width $sJ < D = 2t$ and the filling is incommensurate

- The impurity spins are sufficiently dense $\xi_{cr} < \xi_0 \sqrt{\nu_0 J^2 / T_K}$ and we do not distinguish the lattice constants $\xi_0 \approx \xi_s$

- Work in continuum limit and temperature $T \to 0$

- Physics is dominated by RKKY interactions and we neglect forward scattering

## 2.2. Helical states in 1D Kondo Chain

In this section, we review the main results of Refs. [1,4]. One starts from Eq.(2.1) and linearizes the dispersion relation around its Fermi points. For details see Appendix A. We switch to the Lagrangian description and work in the imaginary time path integral formulation. For a given Hamiltonian the partition function is given by

$$Z = \int \mathcal{D}\{\bar{c}, c\} \exp\left\{ - \int d\{\tau, x\} \, \bar{c} \, \partial_\tau \, c - \mathcal{H}\left[\bar{c}, c\right] \right\}, \tag{2.3}$$

where $\tau$ is imaginary time and $\mathcal{H}$ is the Hamiltonian density. The argument of the exponent is the action $S$ of the system. From now on we use Einstein sum convention for the remainder of the thesis.

The linearized Lagrangian of the free electron part $\mathcal{H}_0$ in Eq.(2.1) reads

$$\mathcal{L}_0 = R_\sigma^\dagger \, \partial_R \, R_\sigma + L_\sigma^\dagger \, \partial_L \, L_\sigma, \quad \partial_{R/L} = \partial_\tau \mp v_F \partial_x, \tag{2.4}$$

where $R^{(\dagger)}, L^{(\dagger)}$ are chiral fields describing the annihilation (creation) of right and left moving fermions. The chiral derivative $\partial_{R/L}$ contains the linearized dispersion of these states. For the Kondo interaction one finds a backscattering term, which contains fast oscillations $\sim 2k_F$.

$$\mathcal{L}_{BS} = R_\sigma^\dagger \left[ \sum_{a=x,y,z} \rho_s J_a \mathbf{S}^a \cdot \boldsymbol{\sigma}_a^{\sigma\sigma'} \right] L_{\sigma'} \, e^{2ik_F x} + h.c., \tag{2.5}$$

The fast oscillations in Eq.(2.5) can be absorbed in the spin configuration of $\mathbf{S}$ which must minimize the ground state energy.

### 2.2.1. Parameterization of the impurity spin $\mathbf{S}_j$

To develop a low energy theory of the Kondo chain, it is necessary to seperate slow degrees of freedom and integrate over the fast ones. Let us explicitly single out the fast $2k_F$ and slow component of the spin field.

$$\frac{\mathbf{S}_j}{s} = \mathbf{m} + [\mathbf{e}_1 \cos(2k_F x + \alpha) + \mathbf{e}_2 \sin(2k_F x + \alpha)] \sqrt{1 - \mathbf{m}^2}, \tag{2.6}$$

where $\{\mathbf{e}_1, \mathbf{e}_2, \mathbf{m}\}$ is an orthogonal triad of vectors, which have smooth coordinate dependence and slow time dependence on a scale of $k_F^{-1}$.
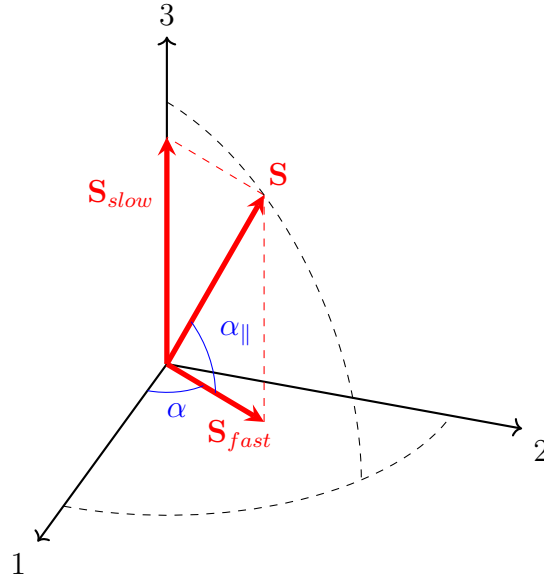


Figure 2.3: The impurity spin can be decomposed into a fast and a slow component. We explicitly single out the fast oscillations in the $\mathbf{e}_1$ and $\mathbf{e}_2$ directions.

We choose $\mathbf{m} = \sin\left(\alpha_\parallel\right)\mathbf{e}_3$ and parameterize $\{\mathbf{e}_1, \mathbf{e}_2, \mathbf{e}_3\}$ with Euler angles

$$\mathbf{e}_1 = \left(-\cos\left(\theta\right)\cos\left(\psi\right), -\cos\left(\theta\right)\sin\left(\psi\right), \sin\left(\theta\right)\right)^T, \tag{2.7}$$

$$\mathbf{e}_2 = \left(\sin\left(\psi\right), -\cos\left(\psi\right), 0\right)^T, \tag{2.8}$$

$$\mathbf{e}_3 = \left(\sin\left(\theta\right)\cos\left(\psi\right), \sin\left(\theta\right)\sin\left(\psi\right), \cos\left(\theta\right)\right)^T. \tag{2.9}$$

The spin is parameterized by four angles, instead of the usual two angles, coming from a parameterization of a vector field in spherical coordinates. However, this will not result in over counting the spin degrees of freedom, since two angles will turn out to be massive, fast fields, which will be integrated out. The low energy theory of the spin will only depend on two angles, thus justifying this approach.

The parameterization in Eq.(2.6) of the spin fulfills the normalization condition $\left|\frac{\mathbf{S}}{s}\right|^2 = 1$. For the parameterization of $\mathbf{S}_j$ in terms of a vector field, one finds an additional contribution to the action called the Wess-Zumino term, which accounts for the quantum nature of the spin, ensuring correct exchange relation and completeness of the spin description, for details see Appendix D. After inserting Eq.(2.6), the Wess-Zumino term is given by

$$\mathcal{L}_{WZ}^{sl} = \frac{is\rho_s}{\xi_0}\sin\left(\alpha_\parallel\right)\left[\partial_\tau\alpha + \cos\left(\theta\right)\partial_\tau\psi\right]. \tag{2.10}$$

Inserting Eq.(2.6) in Eq.(2.5) and keeping only non-oscillating terms gives

$$\mathcal{L}_{BS}^{sl} = \mathrm{R}_\sigma^\dagger \sum_{a=x,y,z} \Delta_a\left[\mathbf{e}_1 + i\,\mathbf{e}_2\right]\cdot\boldsymbol{\sigma}_a^{\sigma\sigma'}e^{-i\alpha}\mathrm{L}_{\sigma'} + h.c., \quad \Delta_a = s\frac{\rho_s}{2}J_a\sqrt{1-\mathbf{m}^2} \tag{2.11}$$

Inserting Eqs. (2.7)–(2.9) into Eq. (2.11) yields

$$\mathcal{L}_{BS}^{sl} = \mathrm{R}_\sigma^\dagger\,\Delta_\perp\left[e^{i\psi}\sin^2\left(\frac{\theta}{2}\right)\sigma_-^{\sigma\sigma'} - e^{-i\psi}\cos^2\left(\frac{\theta}{2}\right)\sigma_+^{\sigma\sigma'}\right]\mathrm{L}_{\sigma'}\,e^{-i\alpha} + $$
$$+ \mathrm{R}_\sigma^\dagger\,\Delta_z\sin\left(\theta\right)\sigma_z^{\sigma\sigma'}\,\mathrm{L}_{\sigma'}\,e^{-i\alpha} + h.c., \tag{2.12}$$

where $\Delta_a = s\frac{\rho_s}{2}J_a\cos\left(\alpha_\parallel\right)$, and $\sigma_\pm = \frac{1}{2}\left(\sigma_x \pm i\,\sigma_-\right)$.

For fixed angles $\theta, \alpha_\parallel$ in Eq. (2.11), the backscattering Lagrangian acts like a mass term for the fermions. Opening a gap reduces the energy of the electrons. The energy gain is calculated in Appendix B and given by

$$\delta F = F(\Delta) - F(0) = -\frac{\xi_0}{\pi v_F}\sum_{\substack{\text{all gapped}\\\text{sectors}}}\Delta^2\log\left(\frac{D}{|\Delta|}\right). \tag{2.13}$$

Minimizing the ground state energy is equivalent to maximizing the fermionic gap. We continue by considering two limiting cases. The Easy Axis phase $J_\perp \to 0$ and the Easy Plane phase $J_z \to 0$.
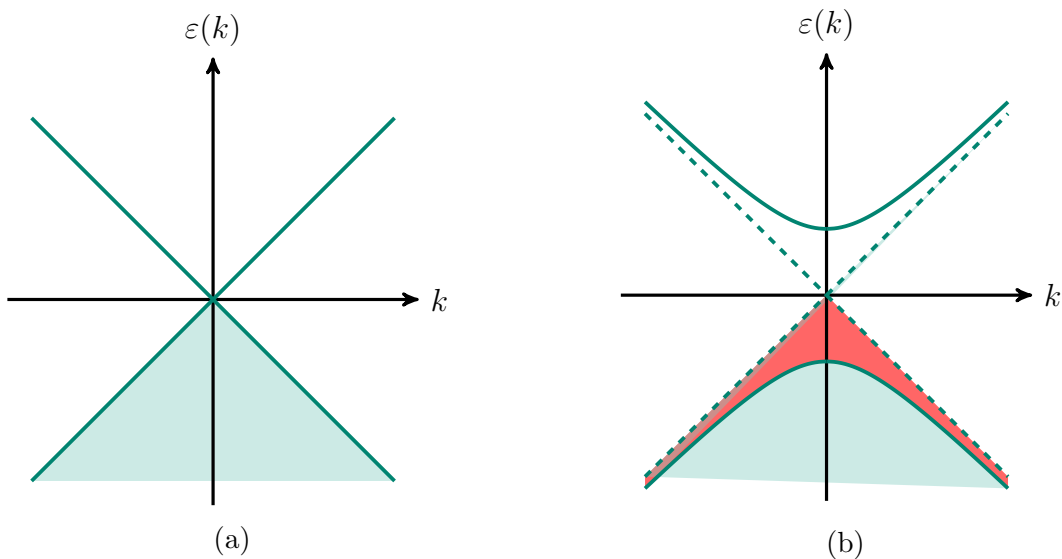
Figure 2.4: The backscattering alters the linear dispersion of Panel (a) and opens a gap, shown in Panel (b). The occupied states below the Fermi level indicated by the light green color move to lower energies in the process of the gap opening. The red area depicts the energy gain, which is the difference of the area under the linear dispersion and the gapped dispersion.

## 2.2.2. Easy Axis anisotropy

Let us consider $J_\perp \to 0$. Equation (2.12) reduces to

$$\mathcal{L}_{BS}^{sl,EA} = \mathrm{R}_\sigma^\dagger \, \Delta \sin(\theta) \, \sigma_z^{\sigma\sigma'} \, \mathrm{L}_{\sigma'} \, e^{-i\alpha} + h.c., \tag{2.14}$$

where $\Delta = \Delta_z = s\frac{\rho_s}{2} J_z \cos(\alpha_\|)$. We proceed by removing the phase $\alpha$ from Eq. (2.14). This can be done either by a gauge transformation of the following form

$$\mathrm{R}_\uparrow \to e^{\frac{-i\alpha}{2}} R_\uparrow, \quad \mathrm{R}_\downarrow \to e^{\frac{-i\alpha}{2}} R_\downarrow, \quad \mathrm{L}_\uparrow \to e^{\frac{+i\alpha}{2}} L_\uparrow, \quad \mathrm{L}_\downarrow \to e^{\frac{+i\alpha}{2}} L_\downarrow \tag{2.15}$$

or by bosonizing the fermionic operators and shifting the bosonic phases by the respective angles. We do the latter, which might seem more cumbersome at first, but does not require calculating the Jacobian of the gauge transformation. The whole procedure is explained in Appendix C. After shifting, the Lagrangian is given by

$$\mathcal{L} = \mathcal{L}_0 + \mathcal{L}_{BS}^{sl,EA}\Big|_{\alpha=0} + \frac{1}{2} \mathcal{L}_{LL}[\alpha, v_F] + \mathcal{L}_{WZ}^{sl}, \tag{2.16}$$

with $\mathcal{L}_{LL}[\phi, v_F] = \frac{1}{2\pi v_F} \left[ (v_F \nabla \phi)^2 + (\partial_\tau \phi)^2 \right]$ being the hydrodynamic action of the Luttinger liquid.

After removing the spin phases one can go back to the fermionic picture. The fermionic gap in Eq. (2.14) is maximal for $\theta = \frac{\pi}{2}$ and $\alpha_\| = 0$. Maximizing the gap

minimizes the ground state energy. The energetically most favorable spin configuration is the one, where all fermions are equally gapped. After integrating out the gapped fermions, Eq. (2.16) is altered by the ground state energy equation Eq. (2.13) and reads as

$$\mathcal{L} = \frac{\delta F}{\xi_0} + \frac{1}{2} \mathcal{L}_{LL}[\alpha, v_F] + \mathcal{L}_{WZ}^{sl}, \tag{2.17}$$

One continues by expanding $\delta F$ and $\mathcal{L}_{WZ}^{sl}$ in leading order in $\theta, \alpha_\parallel$ and integrates out $\theta$ and $\alpha_\parallel$, because they turn out to be massive variables. The remaining fields $\alpha$ and $\psi$ remain massless. For the slow Lagrangian in the Easy Axis phase, one finds

$$\mathcal{L}^{sl,EA} = \frac{1}{2K_\alpha} \mathcal{L}_{LL}[\alpha, v_\alpha], \quad v_\alpha = K_\alpha v_F, \quad K_\alpha \approx \xi_0 \frac{J_z}{\pi v_F} \sqrt{\log\left(\frac{D}{J_z}\right)} \ll 1, \tag{2.18}$$

where we used that the band width $D$ is the largest energy scale of our system $D \gg \frac{v_F}{\xi_0} \gg J_K$. The slow field $\alpha$ couples to charge sources only [1,4]. The transport is thus governed by collective excitations, slow CDWs, which have a strongly renormalized velocity $v_\alpha$ and compressibility $K_\alpha$ due to the interaction with magnetic impurities.

### 2.2.3. Easy Plane anisotropy

Let us now consider the opposing limit $J_z \to 0$, where $\mathcal{L}_{BS}$ takes the following form

$$\mathcal{L}_{BS}^{sl,EP} = R_\sigma^\dagger \Delta \left[ e^{i\psi} \sin^2\left(\frac{\theta}{2}\right) \sigma_-^{\sigma\sigma'} - e^{-i\psi} \cos^2\left(\frac{\theta}{2}\right) \sigma_+^{\sigma\sigma'} \right] L_{\sigma'} e^{-i\alpha} + h.c. \tag{2.19}$$

Here $\Delta = \Delta_\perp = s\frac{\rho_s}{2} J_\perp \cos\left(\alpha_\parallel\right)$. It is convenient to write this as the sum of helical contributions

$$\mathcal{L}_{BS}^{sl(h1)} = -R_\uparrow^\dagger \Delta \cos^2\left(\frac{\theta}{2}\right) e^{-i(\psi+\alpha)} L_\downarrow + h.c., \tag{2.20}$$

$$\mathcal{L}_{BS}^{sl(h2)} = R_\downarrow^\dagger \Delta \sin^2\left(\frac{\theta}{2}\right) e^{i(\psi-\alpha)} L_\uparrow + h.c., \tag{2.21}$$

which are again mass terms for the helical sectors of the $R_\uparrow, L_\downarrow$ and $R_\downarrow, L_\uparrow$ fermions, (if the phases are removed) respectively. By choosing $\theta = \frac{\pi}{2}$, one obtains two gapped helical sectors, both equally gapped with an effective gap $\Delta \cos^2\left(\frac{\pi}{4}\right) = \Delta \sin^2\left(\frac{\pi}{4}\right) = \frac{\Delta}{2}$. According to Eq. (2.13), the ground state energy of this setup is given by

$$\delta F_{\theta=\frac{\pi}{2}} \sim 2 \times -\frac{\Delta^2}{4}, \tag{2.22}$$

where the 2 comes from having a total of two gapped sectors. However, if one chooses $\theta = 0$ or $\theta = \pi$, there is a gapped helical sector with gap $\Delta$ and one ungapped sector.

The ground state energy of this would be proportional to

$$\delta F_{\theta=0,\pi} \sim 1 \times -\Delta^2, \tag{2.23}$$

which gives the lower free energy compared to Eq. (2.22). This means, that spontaneously breaking the $\mathbb{Z}_2$ symmetry between the helical sectors is energetically more favorable than having all fermions equally gapped. There are two possibilities to gap the fermions. Either $R_\uparrow, L_\downarrow$ or $R_\downarrow, L_\uparrow$ acquire a gap. Without a loss of generality we choose $\theta = 0$, which means that the first helical sector $R_\uparrow, L_\downarrow$ is gapped. On the mean field level, the combination $\psi - \alpha$ does not enter the low energy action. In leading order of fluctuations in $\theta$ and $\alpha_\parallel$, the angle $\psi - \alpha$ enters as

$$\mathcal{L} \propto R_\downarrow^\dagger \Delta \left(\frac{\theta}{2}\right)^2 e^{i(\psi-\alpha)} L_\uparrow + h.c. + \frac{is\rho_s}{\xi_0} \alpha_\parallel \frac{\theta^2}{2} \partial_\tau \alpha, \tag{2.24}$$

where the last summand is the slow kinetic term for the spins. We assume that $\alpha_\parallel, \theta \approx 0$. The Wess Zumino Lagrangian also contains a higher order term of $\mathcal{O}(\alpha_\parallel \theta^2)$. The influence of the fluctuations of $\theta$ and $\alpha_\parallel$ can be estimated by integrating over $R_\downarrow$ and $L_\uparrow$, leading to an additional contribution to the action

$$S \propto \text{Tr} \log \left[ \begin{pmatrix} -i\omega + v_F k & \Delta \left(\frac{\theta}{2}\right)^2 e^{i(\psi-\alpha)} \\ \Delta \left(\frac{\theta}{2}\right)^2 e^{i(\psi-\alpha)} & -i\omega - v_F k \end{pmatrix} \right]. \tag{2.25}$$

This can be neglected since the expansion of the logarithm starts only in second order of the gap and gives a contribution $\mathcal{O}(\theta^4)$, which is subleading and beyond our accuracy. Since all relevant expressions and the Wess Zumino term in leading order only depend on the combination of phases $\alpha + \psi$, we can eliminate the phase from $\mathcal{L}_{bs}^{sl(h1)}$ by doing the following shift $\alpha + \psi \to \alpha$ and continue with bosonization and removing the shifted $\alpha$ from the Lagrangian. After integrating out all massive variables, we find

$$\mathcal{L}^{sl,EP} = R_\downarrow^\dagger G_R^{-1} R_\downarrow + L_\uparrow^\dagger G_L^{-1} L_\uparrow + \frac{1}{8K_\alpha'} \mathcal{L}_{LL}[\alpha, v_\alpha'], \tag{2.26}$$

$$K_\alpha' \approx \frac{\xi_0 J_\perp}{2\pi v_F} \sqrt{\log\left(\frac{D}{J_\perp}\right)}. \tag{2.27}$$

The angle $\alpha$ again descibes slow collective excitations. Due to the shift from $\alpha + \psi$ to $\alpha$ it now couples to charge and spin sources and thus a collective helical mode. The interaction with the magnetic impurities strongly renormalize the Fermi velocity $v_\alpha'$ and the compressibility $K_\alpha'$, similar to the Easy Axis case. Additionally one finds free helical fermions, which can be bosonized and form a helical Luttinger liquid.

### 2.2.4. Adding spinless disorder

Let us discuss the transport properties of helical fermions in the Easy Plane phase; for a full detailed analysis, see Refs. [1, 4]. Consider the smooth $2k_F$ component $g$ of a weak random scalar potential. The disorder potential is of the form

$$\mathcal{L}_{\mathrm{dis}} = g(x)\,\mathrm{R}_\sigma^\dagger\,\mathrm{L}_\sigma + h.c. \qquad (2.28)$$

After removing the phase in Eq. (2.20), the phase reappears in Eq. (2.28), but for the sake of the argument, we assume that it takes a constant mean field value and can be neglected. We continue by integrating out the gapped fermions $\mathrm{R}_\uparrow$ and $\mathrm{L}_\downarrow$. We define gapped spinors $\Psi_g = (\mathrm{R}_\uparrow, \mathrm{L}_\downarrow)^T$ and ungapped spinors $\Psi_u = (\mathrm{R}_\downarrow, \mathrm{L}_\uparrow)^T$ and use the identity

$$\left\langle \exp\left( -\int d\tau\,dx\,\left\{ g(x)\Psi_g^\dagger\,\tau_x\,\Psi_u + h.c. \right\} \right) \right\rangle =$$
$$= \exp\left( \frac{1}{2}\int dM \left\{ \left[ g\Psi_u^\dagger \right]_{(x_1,\tau_1)} \tau_x \left[ \left\langle \Psi_g^\dagger \Psi_g \right\rangle_g \right]_{\binom{x_1-x_2,}{\tau_1-\tau_2}} \tau_x \left[ \Psi_u g \right]_{(x_2,\tau_2)} \right\} \right), \quad (2.29)$$

where $M = \{\tau_1, \tau_2, x_1, x_2\}$ and $\tau_x$ is the first Pauli matrix in the chiral space. The gapped Green's function $\left\langle \Psi_g^\dagger \Psi_g \right\rangle_g$ can be computed straightforwardly

$$\mathbf{G}_g = \frac{1}{\Delta^2 - G_R^{-1}G_L^{-1}} \begin{pmatrix} -G_L^{-1} & \Delta \\ \Delta & -G_R^{-1} \end{pmatrix} \approx \begin{pmatrix} 0 & \frac{1}{\Delta} \\ \frac{1}{\Delta} & 0 \end{pmatrix}, \qquad (2.30)$$

where $G_{R(L)}^{-1}$ are the inverse Green's functions of the chiral fermions and we expand the Green's function in $\Delta$. Taking Eq. (2.29) and changing to relative coordinate $x_{1/2} = x \pm \frac{\Delta x}{2}$, with similar relations for $\tau$, gives

$$S_{dis} = -\frac{1}{2}\int dM' \left[ g\Psi_u^\dagger \right]_{\left(x+\frac{\Delta x}{2}, \tau+\frac{\Delta\tau}{2}\right)} \tau_x \left[ \left\langle \Psi_g^\dagger \Psi_g \right\rangle_g \right]_{(\Delta x, \Delta\tau)} \tau_x \left[ \Psi_u g \right]_{\left(x-\frac{\Delta x}{2}, \tau-\frac{\Delta\tau}{2}\right)} \approx$$
$$\approx -\int \{d\tau, dx\}\,\frac{g(x)^2}{2\Delta}\,\mathrm{R}_\downarrow^\dagger\,\mathrm{L}_\uparrow + h.c., \quad (2.31)$$

where $M' = \{\tau, \Delta\tau, x, \Delta x\}$ and $\Psi' = \tau_x \Psi$. In the last step we used that the Green's function is short-ranged on a time scale of $\Delta^{-1}$ or beyond the correlation length $\xi_{EP} = \frac{v_F}{\Delta}$, respectively. This means that two slow fields connected by the gapped Green's function form a single local field on length- and timescales large compared to the inverse gap. The ungapped fermionic action is altered by

$$\mathcal{L}_{\mathrm{dis}}^{\mathrm{eff}} = -\frac{g(x)^2}{2\Delta}\,\mathrm{R}_\downarrow^\dagger\,\mathrm{L}_\uparrow + h.c. \qquad (2.32)$$

Single particle backscattering processes on the spinless impurities are impossible. Multiparticle processes involving the Kondo impurities are possible, but for a large fermionic gap $\Delta \gg g$ are parametrically suppressed. This means, that the transport carried by the gapless helical fermions is ballistic up to parametrically large scales.

## 2.3. Statement of the problem

We have already discussed various physical systems where helical states can emerge. Magnetically doped 1D quantum wires, theoretically described by a Kondo chain, can host helical states under certain conditions. However, it was unclear whether one dimensionality is strictly needed to find such helical states in experiment. The scope of this thesis is to find conditions under which a quasi-one dimensional helical phase can also be found in samples consisting of a small number of coupled magnetically doped wires.

A signature of a global (quasi-one dimensional) helical phase is found if there is a lock-in relation between the electron's spin and momentum in all conducting channels. This results for example in a non-zero spin current without an applied bias voltage, see Fig. 2.5. We also adress the question if the helical phase inherits the protected transport properties from the one dimensional one.
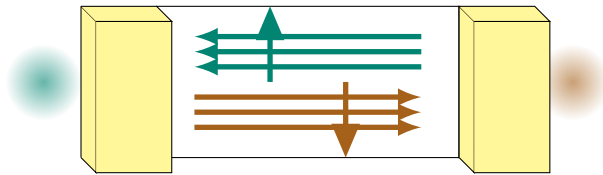


Figure 2.5: A schematic setup showing a global helical phase in a Quasi-1D sample.

A hint for a global helical ordering would make helical states in magnetically doped quantum wires much more accessible for a wider class of experimental test, which have not been considered before.

# 3

# Quasi-1D Kondo chain

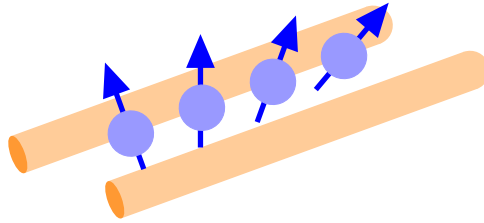## 3.1. Two 1D wires coupled to one impurity chain



Figure 3.1: Two channels of itinerant electrons (orange) coupled to one chain of impurities (blue). Electrons can directly hop from one channel to the other or interact with the impurities in each channel, respectively.

The easiest setup one might think of consists of two 1D systems of itinerant electrons which are coupled to one impurity chain, see Fig.3.1. However, this setup is trivial, since once the helical order of the impurity spins is established, it will gap out the same helical sector for both itinerant electron systems. Which fermions are gapped is determined by spontaneous symmetry breaking of the $\mathbb{Z}_2$ symmetry of the helical fermions. All assumptions about helical states hold and the global helicity can emerge.

This can easily be seen if one considers two modes, which are not directly tunnel coupled at first. This means, that we can estimate the optimal spin configuration of each wire individually. We label the fermions in each wire with an orbital index $f = 1, 2$, respectively. From Eqs. (2.20) and (2.21) we find

$$\mathcal{L}_{BS}^{sl(h1)} = - \mathrm{R}_{f\uparrow}^\dagger \, \Delta \cos^2\left(\frac{\theta}{2}\right) e^{-i(\psi+\alpha)} \, \mathrm{L}_{f\downarrow} + h.c., \tag{3.1}$$

$$\mathcal{L}_{BS}^{sl(h2)} = \mathrm{R}_{f\downarrow}^\dagger \, \Delta \sin^2\left(\frac{\theta}{2}\right) e^{i(\psi-\alpha)} \, \mathrm{L}_{f\uparrow} + h.c., \tag{3.2}$$

Note, that the angles $\theta, \Psi, \alpha$ are the same for both wires, because they couple to the same impurity chain. This means, that we can only gap $R_{1\uparrow}, L_{1,\downarrow}, R_{2\uparrow}, L_{2\downarrow}$ or $R_{1\downarrow}, L_{1,\uparrow}, R_{2\downarrow}, L_{2\uparrow}$. Since turning on the coupling does not favor a given helicity we

can expect in this case, that both wires will support fermions with either $h_1 = +1$ & $h_2 = +1$ or $h_1 = -1$ & $h_2 = -1$ with the same probability. We will thus find a global helical phase in this system.

## 3.2. Two coupled Kondo chains

Let us consider two coupled Kondo chain, consisting of one conduction channel and one impurity chain each, see Fig.3.2. In contrast to Section 3.1 we now doubled the spin degrees of freedom. A helical state may form in each wire individually. Electrons, tunneling between the wires, can now mediate a feedback of one impurity spin chain to the other. This is significantly different from Section 3.1, because if one finds a helical phase, it is not automatically a global one.
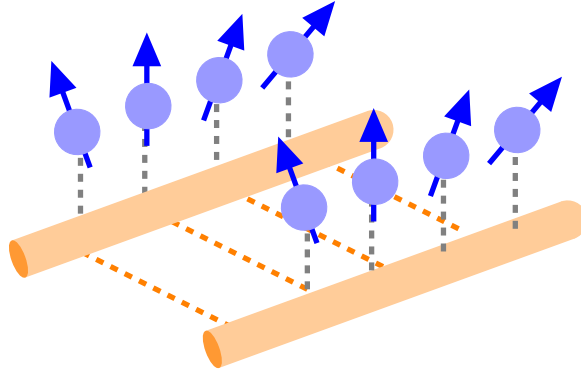


Figure 3.2: Two Kondochains which are coupled by tunneling. Each KC consists of one conduction channel and a chain of magnetic impurities.

The Hamiltonian of such a system is given by

$$\mathcal{H} = \mathcal{H}_{KC,1} + \mathcal{H}_{KC,2} + \underbrace{\sum_{j,\sigma} \left( -t_\perp \, c_{j,1}^\dagger \, c_{j,2} + h.c. \right)}_{\mathcal{H}_\perp}, \tag{3.3}$$

$$\mathcal{H}_{KC} = \underbrace{\sum_{j,f,\sigma} -t \left( c_{j+1,f,\sigma}^\dagger \, c_{j,f,\sigma} + h.c. \right)}_{\mathcal{H}_0} + \underbrace{\sum_{a,m\in M,f,\sigma,\sigma'} J_a \, c_{m,f,\sigma}^\dagger \, \mathbf{S}_{m,f}^a \cdot \boldsymbol{\sigma}_a^{\sigma\sigma'} \, c_{m,f,\sigma'}}_{\mathcal{H}_{KI}} . \tag{3.4}$$

Here $t$ and $t_\perp$ are the intra- and interchain hopping strength, $c_{j,f,\sigma}^\dagger (c_{j,f,\sigma})$ creates (annihilates) an electron at lattice site $j$ in wire $f = 1, 2$ with $\sigma = \uparrow, \downarrow$, $\mathbf{S}_{j,f}$ is a spin $s$ magnetic impurity localized at lattice site $j$ in wire $f$, $\sigma_a$ denotes Pauli matrices which act on the spin degree of freedom and M constitutes a subset of all lattice sites. $J_a$ describes the strength of the interaction between itinerant electrons and magnetic impurities.

We start by setting $J_a = 0$ and diagonalize Eq. (3.3). Using the relations for the Fourier transform Eqs. (A.1) and (A.2), we find a dispersion relation describing two bands

$$\varepsilon_\pm = -2t\cos(k\xi_0) \mp t_\perp. \tag{3.5}$$

We use the diagonalizing transformation $c_{1/2} = \frac{1}{\sqrt{2}}\left[c_+ \pm c_-\right]$ on Eq. (3.3) and switch to the Lagrangian formulation as before. This gives

$$\mathcal{L} = \sum_{a,\nu=\pm} \left[ c_\nu^\dagger\, \varepsilon_\nu\, c_\nu + \frac{J_a}{2}\left( c_\nu^\dagger\, \mathbf{S}_{+a}\boldsymbol{\sigma}_a\, c_\nu + c_\nu^\dagger\, \mathbf{S}_{-a}\boldsymbol{\sigma}_a\, c_{-\nu} + h.c. \right) \right], \tag{3.6}$$

where $\mathbf{S}_\pm = \mathbf{S}_1 \pm \mathbf{S}_2$. The model described by Eq. (3.6), describes two bands, which are split by the tunneling. The orignal Kondo interaction was diagonal in the "wire"-space. However, after applying the transformation, which diagonalizes $\mathcal{H}_0 + \mathcal{H}_\perp$, we find intraband scattering $\sim \mathbf{S}_+$ and interband scattering $\sim \mathbf{S}_-$ terms.

We distinguish the three relevant cases shown in Fig. 3.3. In Panel (a), the two bands are just weakly split by the tunneling. The Fermi momentum, corresponding to the respective Fermi points, is of the same order $k_{F_+} \approx k_{F_-}$, and one can treat the splitting perturbatively in $t_\perp$. In Panel (b), the splitting is larger, but on the level of the chemical potential one still finds four Fermi points, which now have Fermi momenta of different magnitude $k_{F_-} < k_{F_+}$. This implies that the difference $k_{F_+} - k_{F_-}$ is of order $\mathcal{O}(k_F)$ and oscillations depending on this difference can be neglected. In Panel (c), the tunneling is strong and one has two separated bands. To account for tunneling processes, which may lead to renormalization of physical quantities, one can pertubatively integrate out the upper band as a function of $t_\perp^{-1}$.
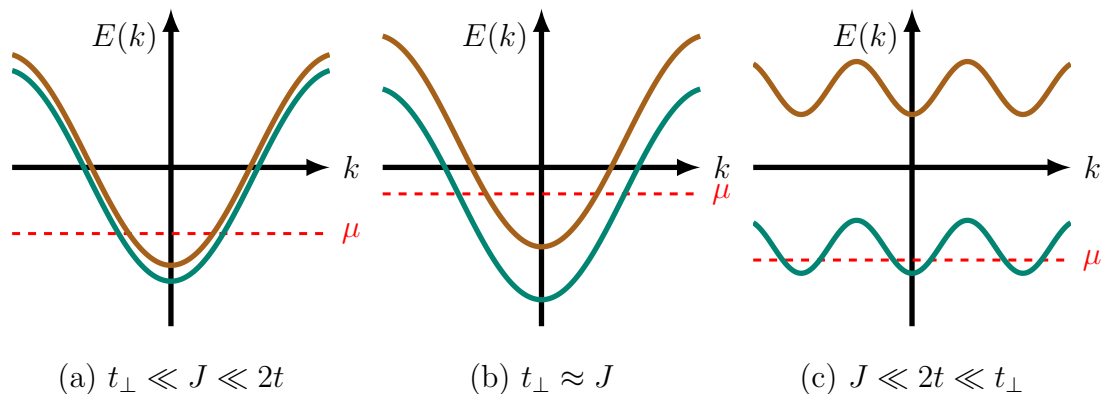


Figure 3.3: Three physically different cases. Panel (a): The two wires are only weakly coupled $t_\perp \ll J \ll 2t$. The tunneling $t_\perp$ can be treated as a small pertubation. Panel (b): The tunneling is of the same magnitude as the Kondo interaction $t_\perp \approx J_K$. On the level of the chemical potential all backscattering processes have to be taken into account in order to find the optimal spin configuration. Panel (c): There are two well seperated bands and the chemical potential is in the lower wire. The upper band can be integrated out perturbatively by using the smallness of the ratio $\sim \frac{J}{t_\perp}$

## 3.3. Weakly coupled chains

In this section, we set $J_z = 0$ and analyze the situation, where the tunneling only weakly splits the bands $t_\perp \ll J \ll 2t$. In this regime, the Fermi momenta are roughly of the same order $k_{F_+} \approx k_{F_-}$. We linearize the dispersion around the Fermi points $k_{F_{+(-)}}$, corresponding to the lower(upper bands). This gives

$$\varepsilon_\pm|_{k=k_{F_\pm}} \approx -2t \cos\left(k_{F_\pm}\xi_0\right) - t_\perp + 2t\xi_0 \sin\left(k_{F_\pm}\xi_0\right)\left(k - k_{F_\pm}\right), \qquad (3.7)$$

$$\varepsilon_\pm|_{k=-k_{F_\pm}} \approx -2t \cos\left(k_{F_\pm}\xi_0\right) + t_\perp - 2t\xi_0 \sin\left(k_{F_\pm}\xi_0\right)\left(k + k_{F_\pm}\right). \qquad (3.8)$$
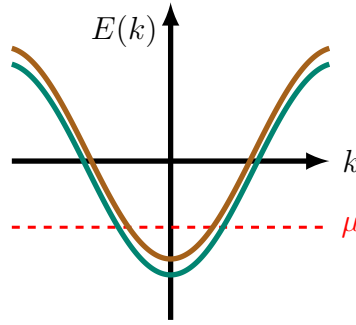


$$t_\perp \ll J \ll 2t$$

Figure 3.4: Bandstructure for weakly split bands $t_\perp \ll J \ll 2t$. We assume the chemical potential is placed such, that we find four Fermi points.

The constant terms of the expansion must be absorbed in the chemical potential, which allows us to determine $\delta k_F = k_{F_+} - k_{F_-}$.

$$\mu = -2t \cos\left(k_{F_+}\xi_0\right) - t_\perp \stackrel{!}{=} -2t \cos\left(k_{F_-}\xi_0\right) + t_\perp \qquad (3.9)$$

$$2t_\perp = 4t \sin\left(k_F\xi_0\right) \sin\left(\frac{\delta k_F}{2}\xi_0\right), \qquad (3.10)$$

where we introduced the mean $\tilde{k}_F = \frac{1}{2}\left(k_{F_+} + k_{F_-}\right)$ and difference $\delta k_F = k_{F_+} - k_{F_-}$. For the splitting of the bands we find

$$\delta k_F = \frac{2}{\xi_0} \arcsin\left(\frac{t_\perp \xi_0}{v_F}\right) \approx \frac{2t_\perp}{v_F}, \qquad (3.11)$$

where we expanded in $t_\perp$ in the last step and used the definition of $v_F = 2t\xi_0 \sin\left(k_F\xi_0\right)$. Let us continue with Eq. (3.6) and single out smooth left and right moving modes for the four Fermi points of the upper band $\pm k_{F_-}$ and the lower band $\pm k_{F_+}$.

$$c_{\pm,\sigma} = e^{-ik_{F_\pm}x} R_{\pm,\sigma} + e^{ik_{F_\pm}x} L_{\pm,\sigma}. \qquad (3.12)$$

Here $c_\pm^{(\dagger)}$ is the field corresponding to the annihilation (creation) of chiral fermions in the $\pm$ bands. We select only the backscattering terms in the Kondo interaction and find

$$\mathcal{L} = \sum_{a,\nu=\pm} \left[ \mathrm{R}_\nu^\dagger \, \partial_{R_\nu} \, \mathrm{R}_\nu + \mathrm{L}_\nu^\dagger \, \partial_{L_\nu} \, \mathrm{L}_\nu + \right.$$
$$\left. + \frac{J_a}{2} \left( \mathrm{R}_\nu^\dagger \, \mathbf{S}_{+_a} \boldsymbol{\sigma}_a \, \mathrm{L}_\nu \, e^{2ik_{F_\nu}x} + \mathrm{R}_\nu^\dagger \, \mathbf{S}_{-_a} \boldsymbol{\sigma}_a \, \mathrm{L}_{-\nu} \, e^{i(k_{F_+}+k_{F_-})x} + h.c. \right) \right], \quad (3.13)$$

where $\partial_{R/L_\nu} = \partial_\tau \mp i v_{F_\nu} \partial_x$ is the chiral derivative with the Fermi velocity $v_{F_\pm}$ corresponding to the bands. Note, that one finds intraband backscattering oscillating with either $\sim k_{F_+}$ or $\sim k_{F_-}$. The interband backscattering always oscillates with the combination $\sim k_{F_+} + k_{F_-}$. This can be easily seen from Fig. 3.5, which shows possible backscattering processes and their corresponding Fermi momenta. We use the definitions $\tilde{k}_F = \frac{1}{2} \left( k_{F_+} + k_{F_-} \right)$ and $\delta k_F = k_{F_+} - k_{F_-}$. Because $k_{F_\pm}$ are of the same magnitude, $\tilde{k}_F$ is large and we absorb it in our spin configuration and $\delta k_F$ remains small. We can fully absorb the interband oscillations into our spin configuration. For the intraband oscillations we absorb only $\tilde{k}_F$, which leaves the gaps slowly oscillating. We parameterize the spins in the following way

$$\frac{\mathbf{S}_\pm}{s} = \mathbf{m}_1 \pm \mathbf{m}_2 + \left[ \mathbf{e}_1^{(1)} \sqrt{1 - \mathbf{m}_1^2} \pm \mathbf{e}_1^{(2)} \sqrt{1 - \mathbf{m}_2^2} \right] \cos\left( 2\tilde{k}_F x \right) +$$
$$+ \left[ \mathbf{e}_2^{(1)} \sqrt{1 - \mathbf{m}_1^2} \pm \mathbf{e}_2^{(2)} \sqrt{1 - \mathbf{m}_2^2} \right] \sin\left( 2\tilde{k}_F x \right), \quad (3.14)$$

where we inserted the parameterization of Eq. (2.6) for the single spins $\mathbf{S}_{1/2}$ into the definition of our composite spins. Inserting Eq. (3.14) in Eq. (3.13) and keeping only the slowly oscillating terms gives for the intraband scattering

$$\mathcal{L}_{BS}^{\pm\pm} = \tilde{J}_a \, \mathrm{R}_\pm^\dagger \left[ \sqrt{1 - \mathbf{m}_1^2} \left[ \mathbf{e}_1^{(1)} + i \, \mathbf{e}_2^{(1)} \right]_a \cdot \boldsymbol{\sigma}_a + \right.$$
$$\left. + \sqrt{1 - \mathbf{m}_2^2} \left[ \mathbf{e}_1^{(2)} + i \, \mathbf{e}_2^{(2)} \right]_a \cdot \boldsymbol{\sigma}_a \right] \mathrm{L}_\pm \, e^{\mp i \delta k_F x} + h.c., \quad (3.15)$$

And for the interband scattering

$$\mathcal{L}_{BS}^{\pm\mp} = \tilde{J}_a \, \mathrm{R}_\pm^\dagger \left[ \sqrt{1 - \mathbf{m}_1^2} \left[ \mathbf{e}_1^{(1)} + i \, \mathbf{e}_2^{(1)} \right]_a \cdot \boldsymbol{\sigma}_a - \right.$$
$$\left. - \sqrt{1 - \mathbf{m}_2^2} \left[ \mathbf{e}_1^{(2)} + i \, \mathbf{e}_2^{(2)} \right]_a \cdot \boldsymbol{\sigma}_a \right] \mathrm{L}_\mp + h.c., \quad (3.16)$$

with $\tilde{J}_a = s\frac{\rho_s}{2} J_a$. In general we can have three different relevant types of scattering, see Fig. 3.5. Since our composite spins $\mathbf{S}_\pm$ are linear combination of the original spins $\mathbf{S}_{1/2}$, we expect the gap values in our $\pm$-basis to also linearly depend on the gap values in the $1/2$ basis. The intraband scattering governed by $\mathbf{S}_+ = \mathbf{S}_1 + \mathbf{S}_2$ will depend on the sum of the orignal gaps in the wire space. The interband scattering
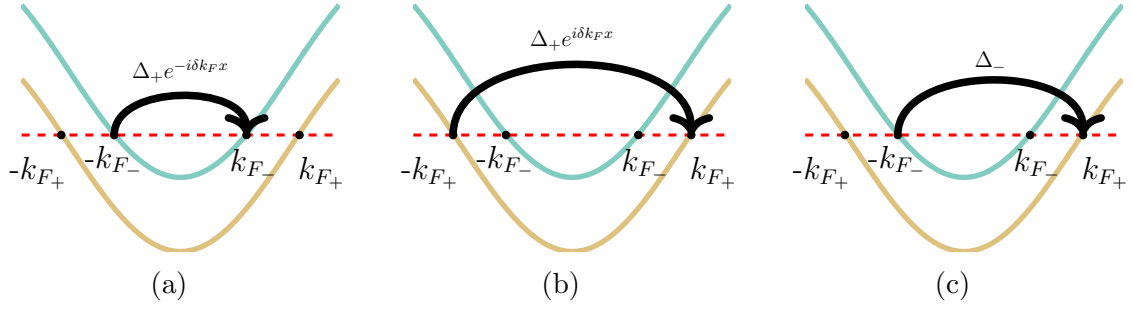
Figure 3.5: There are three possible types of backscattering in our system. We schematically depicted here the scattering from a left to a rightmover. Panel(a) shows the intraband scattering process in the upper band. Since the Fermi momentum, which we absorbed into the spin configuration is larger than $k_{F_-}$, we find residual oscillations $\sim -\delta k_F$. Panel(b) shows the same process for the lower band. Here the absorbed momentum is smaller than $k_{F_+}$, which also leads to oscillations $\sim \delta k_F$. Panel (c) shows the interband scattering process, which is not oscillating.

governed by $\mathbf{S}_+ = \mathbf{S}_1 + \mathbf{S}_2$ thus depends on the difference of the original gaps in the wire space. We continue by inserting Eqs. (2.7)–(2.9) into Eqs. (3.15) and (3.16). It is convenient to split up the backscattering Lagrangian into different helical sectors, like we did for the 1D analysis. For the intraband scattering we find

$$\mathcal{L}_{BS}^{\pm\pm(h1)} = R_{\pm\uparrow}^\dagger \left[ \Delta_+^{(h1)} \right] L_{\pm\downarrow} \, e^{\pm i\delta k_F x} + h.c., \tag{3.17}$$

$$\mathcal{L}_{BS}^{\pm\pm(h2)} = R_{\pm\downarrow}^\dagger \left[ \Delta_+^{(h2)} \right] L_{\pm\uparrow} \, e^{\pm i\delta k_F} + h.c., \tag{3.18}$$

and for the interband scattering we find

$$\mathcal{L}_{BS}^{\pm\mp(h1)} = R_{\pm\uparrow}^\dagger \left[ \Delta_-^{(h1)} \right] L_{\mp\downarrow} + h.c., \tag{3.19}$$

$$\mathcal{L}_{BS}^{\pm\mp(h2)} = R_{\pm\downarrow}^\dagger \left[ \Delta_-^{(h2)} \right] L_{\mp\uparrow} + h.c., \tag{3.20}$$

were the gap values are given by

$$\Delta_\pm^{(h1)} = -\tilde{J} \left[ \cos\left(\alpha_{\|1}\right) e^{-i\psi_1} \cos^2\left(\frac{\theta_1}{2}\right) \pm \cos\left(\alpha_{\|2}\right) e^{-i\psi_2} \cos^2\left(\frac{\theta_2}{2}\right) \right], \tag{3.21}$$

$$\Delta_\pm^{(h2)} = \tilde{J} \left[ \cos\left(\alpha_{\|1}\right) e^{-i\psi_1} \sin^2\left(\frac{\theta_1}{2}\right) \pm \cos\left(\alpha_{\|2}\right) e^{-i\psi_2} \sin^2\left(\frac{\theta_2}{2}\right) \right], \tag{3.22}$$

$$\tilde{J} = \frac{s\rho_s}{2} J_\perp. \tag{3.23}$$

Similar to our previous analysis of the 1D Kondo chain, it will be favorable to break the helical symmetry between the sectors $h1$ and $h2$.

### 3.3.1. Helical phase

Let us consider $\alpha_{\parallel 1} = \alpha_{\parallel 2} = 0$ and choose $\theta_1 = 0$, $\theta_2 = 0$. For the uncoupled wires, we find, that both wires host helical gapless fermions with helicity $h = -1$.
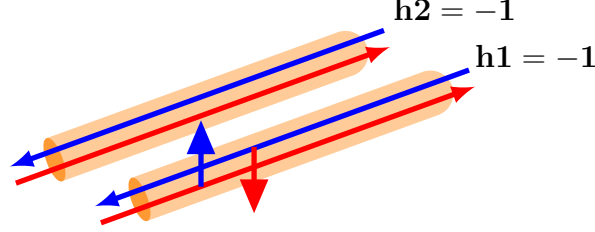


Figure 3.6: For weakly coupled chains, the qualitative picture of uncoupled wires remains valid. We thus find two wires which have helicity $h = -1$.

The corresponding Green's function including tunneling is given by

$$
-\mathbf{G}_{00}^{-1} = \left(
\begin{array}{cccc:cccc}
\partial_{R_+} & \Delta_+ e^{i\delta k_F x} & 0 & \Delta_- & 0 & 0 & 0 & 0 \\
\Delta_+^\dagger e^{-i\delta k_F x} & \partial_{L_+} & \Delta_-^\dagger & 0 & 0 & 0 & 0 & 0 \\
0 & \Delta_- & \partial_{R_-} & \Delta_+ e^{-i\delta k_F x} & 0 & 0 & 0 & 0 \\
\Delta_-^\dagger & 0 & \Delta_+^\dagger e^{i\delta k_F x} & \partial_{L_-} & 0 & 0 & 0 & 0 \\
\hdashline
0 & 0 & 0 & 0 & \partial_{R_+} & 0 & 0 & 0 \\
0 & 0 & 0 & 0 & 0 & \partial_{L_+} & 0 & 0 \\
0 & 0 & 0 & 0 & 0 & 0 & \partial_{R_-} & 0 \\
0 & 0 & 0 & 0 & 0 & 0 & 0 & \partial_{L_-}
\end{array}
\right)
\begin{array}{l}
R_{+\uparrow} \\ L_{+\downarrow} \\ R_{-\uparrow} \\ L_{-\downarrow} \\ \\ R_{+\downarrow} \\ L_{+\uparrow} \\ R_{-\downarrow} \\ L_{-\uparrow}
\end{array}, \quad (3.24)
$$

where the scattering amplitudes are reduced to $\Delta_\pm = -\frac{\tilde{J}}{2}\left(e^{-i\psi_1} \pm e^{-i\psi_2}\right)$ and the ordering of the states is indicated to the right. The slow oscillations in the upper left block can be removed by a gauge transformation of the following form:

$$
R_{\pm\uparrow} \to R_{\pm\uparrow}\, e^{\pm i \frac{\delta k_F}{2} x}, L_{\pm\downarrow} \to L_{\pm\downarrow}\, e^{\mp i \frac{\delta k_F}{2} x}. \quad (3.25)
$$

The removal of the oscillations leads to a shift in the chemical potential of the rotated fermions. In this setup, the fermions $R_{\pm\downarrow}$ and $L_{\pm\uparrow}$ are gapless. The fermions $R_{\pm\uparrow}$ and $L_{\pm\downarrow}$ appear to be gapped with an off diagonal contributions, but now at a nonzero chemical potential, see Eq. (B.7). The Lagrangian of the shifted gapped fermions reads

$$
\mathcal{L}' = \mathcal{L}_0 + \mathcal{L}_{BS}^{\pm\pm(h1)}\Big|_{\delta k_F=0} \pm \frac{v_{F_\pm}\delta k_F}{2}\left(R_{\pm\uparrow}^\dagger R_{\pm\uparrow} + L_{\pm\downarrow}^\dagger L_{\pm\downarrow}\right), \quad (3.26)
$$

where the chemical potential is shifted upwards for the upper band $(-)$ fermions and downwards for the lower band $(+)$ fermions. In the following, we discuss only the upward shift of the upper band fermions, but the downward shift can be discussed similarly. States which have an energy $0 < \varepsilon < \frac{v_{F_-}\delta k_F}{2}$ are pushed above the gap
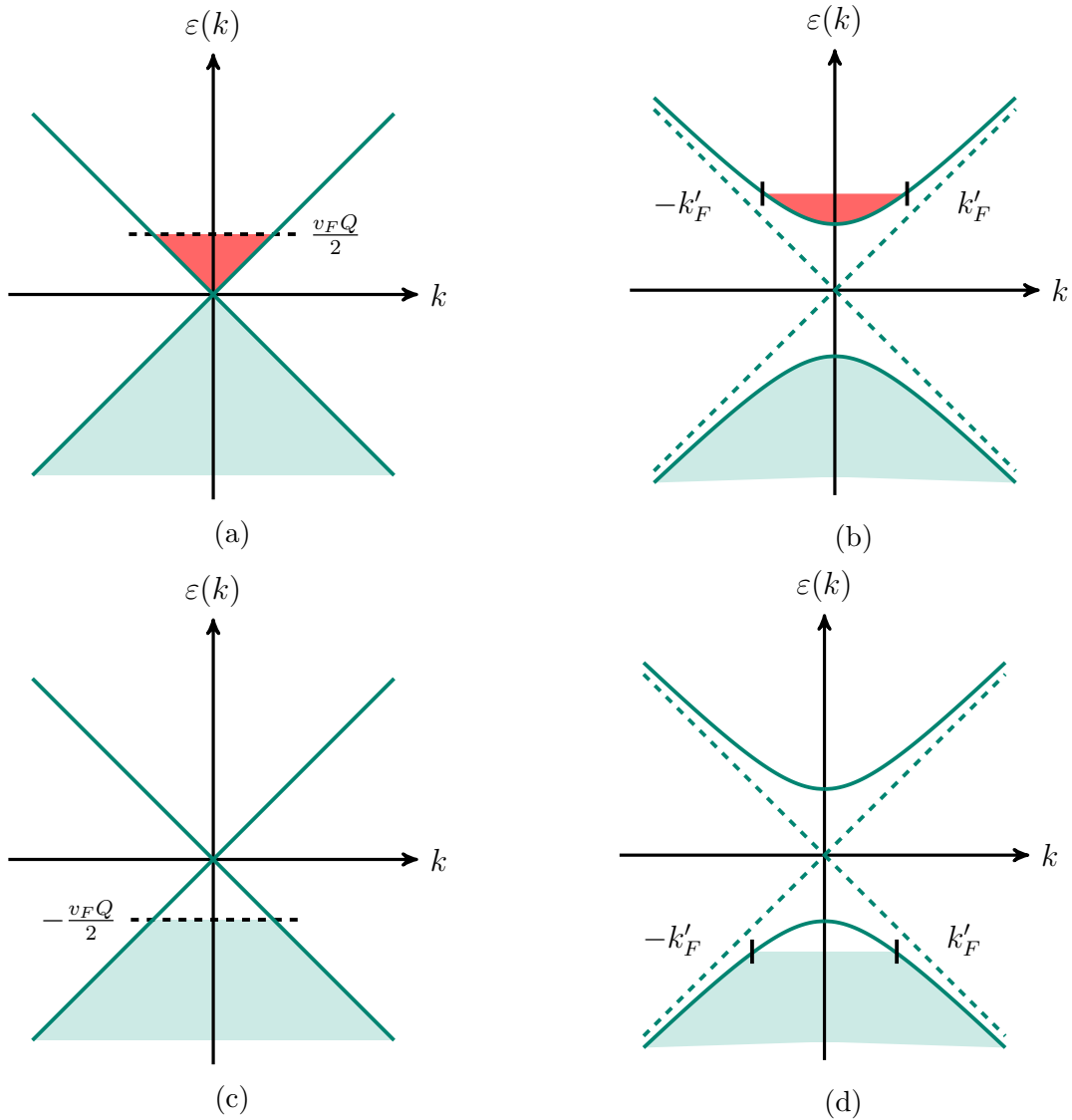
Figure 3.7: Schematic illustration of the gap opening at non-zero chemical potential. In Panel (a), the chemical potential was shifted upwards. In a small region between $0 < E < \frac{v_F Q}{2}$ one now finds occupied states above the Dirac point. After opening the gap, the fermions residing in the upper band are pushed to higher energies, see Panel (b). Since the upper band is only partially filled, one finds a metal, which is governed by a small number of fermions with an almost quadratic dispersion. The same is shown in Panel (c) and Panel (d) for a downward shift. The downward shift results in a hole conducting metallic state.

opened by the backscattering, see Fig. 3.7(b). After opening the gap one finds a small number of fermions in the upper band. The band is only partially filled, thus resulting in a metallic state. The fermions are almost free and have a quadratic dispersion given by

$$\varepsilon_q \approx |\tilde{J}| + \frac{v_{F_-}^2 k^2}{2|\tilde{J}|}. \tag{3.27}$$

Populating states in the upper band after opening the gap leads to an increase in the potential energy of the fermions given by the red area in Fig. 3.7(b).

$$E_{pot} = \xi_0 \int \frac{dk}{2\pi} \varepsilon_q = \frac{\xi_0}{\pi} |\tilde{J}| k'_F + \xi_0 \frac{v_{F_-}^2 k'^3_F}{6\pi |\tilde{J}|}. \tag{3.28}$$

Increasing the tunneling will increase $k'_F = \frac{\delta k_F}{2}$. Pushing up the fermions is favorable, as long as the gain in energy from opening the gap $E_{gap}$ is larger than the cost of potential energy. From this we can compute the critcal value of the tunneling, for which the weak tunneling description is valid in leading order of $t_\perp$.

$$E_{gap} \stackrel{!}{=} E_{pot} \quad \rightarrow \quad \frac{\xi_0}{\pi} \tilde{J} \frac{\delta k_F}{2} \stackrel{!}{=} \frac{\xi_0}{\pi v_F} \tilde{J}^2 \quad \xrightarrow{\delta k_F = \frac{2t_\perp}{v_F}} \quad t_{\perp,\mathrm{crit}} \approx \tilde{J}. \tag{3.29}$$

For tunneling $t_\perp$ of the same strength as the Kondo interaction $\tilde{J}$, the weak tunneling picture breaks down and one cannot assume, that $k_{F_+}$ and $k_{F_-}$ are of the same order. The same analysis holds true for the downward shift of chemical potential. The more the fermions are pushed down, the lesser the influence of the gap opening on the ground state energy becomes. This symmetry between upward and downward shift reflects the electron-hole symmetry of the system. Instead of electron conducting states one finds hole conducting states. However, neither the states above nor below the gap can influence the transport properties of the gapless helical modes at zero chemical potential, because after opening the gap, the gapless states and the almost free fermions are split-off by the gap energy $|\tilde{J}|$.

We proceed by analyzing the contribution to the ground state energy of the gapped fermions. The amplitudes for intra- and interband scattering $\Delta_\pm = -\frac{\tilde{J}}{2}\left(e^{-i\psi_1} \pm e^{-i\psi_2}\right)$ in Eq. (3.24) depend on the spin phases $\psi_1$ and $\psi_2$ in a nontrivial way. We define the new phases

$$\tilde{\psi} = \frac{1}{2}\left(\psi_1 + \psi_2\right), \quad \delta\psi = \psi_1 - \psi_2. \tag{3.30}$$

This allows us to single out a common phase factor in the following way

$$\Delta_\pm = -\frac{\tilde{J}}{2} e^{-i\tilde{\psi}} \left(e^{-i\frac{\delta\psi}{2}} \pm e^{i\frac{\delta\psi}{2}}\right). \tag{3.31}$$

The phase factor $\tilde{\psi}$ can be removed with a gauge transformation or by bosonization, see Appendix C.

$$R_{\pm\downarrow} \rightarrow R_{\pm\downarrow} e^{i\frac{\tilde{\psi}}{2}}, \quad L_{\pm\downarrow} \rightarrow L_{\pm\downarrow} e^{-i\frac{\tilde{\psi}}{2}}. \tag{3.32}$$

This transformation leads to a chiral anomaly like the gauge transformations in Eq. (2.15). The effect of these transformations will be discussed in Section 3.5. To compute the ground state energy of this setup we use Eq. (B.4) and decompose Eq. (3.24) into three parts: The free Green's function $\mathbf{G}_0^{-1}$, which contains all chiral derivatives and the gaps

$$
\mathbf{\Delta} = \underbrace{\begin{pmatrix} 0 & \Delta_+ & 0 & 0 \\ \Delta_+^\dagger & 0 & 0 & 0 \\ 0 & 0 & 0 & \Delta_+ \\ 0 & 0 & \Delta_+^\dagger & 0 \end{pmatrix}}_{\mathbf{\Delta}_+} + \underbrace{\begin{pmatrix} 0 & 0 & 0 & \Delta_- \\ 0 & 0 & \Delta_-^\dagger & 0 \\ 0 & \Delta_- & 0 & 0 \\ \Delta_-^\dagger & 0 & 0 & 0 \end{pmatrix}}_{\mathbf{\Delta}_-}.
\tag{3.33}
$$

Due to the offdiagonal structure of $\mathbf{\Delta}_-$ the gap expansion in Eq. (B.4) seperates

$$
\delta F = -\frac{T}{2} \operatorname{Tr} \mathbf{G}_0 \mathbf{\Delta}_+ \mathbf{G}_0 \mathbf{\Delta}_+ - \frac{T}{2} \operatorname{Tr} \mathbf{G}_0 \mathbf{\Delta}_- \mathbf{G}_0 \mathbf{\Delta}_-,
\tag{3.34}
$$

and we find that the ground state energy can be computed as the sum of all gapped sectors individually. This gives for the ground state energy $\delta F_{\theta_1 \theta_2}$:

$$
\begin{aligned}
\delta F_{00} &= \frac{-\xi_0}{2\pi} \left[ \frac{|\mathbf{\Delta}_+|^2}{v_{F_+}} + \frac{|\mathbf{\Delta}_+|^2}{v_{F_-}} + \frac{4|\mathbf{\Delta}_-|^2}{v_{F_+} + v_{F_-}} \right] \log\left(\frac{D}{|\Delta|}\right) = \\
&= \frac{-\xi_0}{2\pi} \left[ \frac{(v_{F_+} + v_{F_-})^2 + (v_{F_-} - v_{F_+})^2 \cos(2\delta\psi) + 4 v_{F_-} v_{F_+}}{2 v_{F_-} v_{F_+} (v_{F_-} + v_{F_+})} \right] \Delta^2 \log\left(\frac{D}{|\Delta|}\right),
\end{aligned}
\tag{3.35}
$$

which depends on the relative angle between the spin phases $\psi_1 - \psi_2$ and is maximal for $\psi_1 - \psi_2 = 0$. We insert the definition of $v_{F_\pm}$ and compute the ground state energy to leading order in $\delta k_F$ and the tunneling respectively. We find

$$
\begin{aligned}
\delta F_{00} &= \frac{-\xi_0}{2\pi} \left[ \frac{(v_{F_+} + v_{F_-})^2 + (v_{F_-} - v_{F_+})^2 + 4 v_{F_-} v_{F_+}}{2 v_{F_-} v_{F_+} (v_{F_-} + v_{F_+})} \right] \Delta^2 \log\left(\frac{D}{|\Delta|}\right) \approx \\
&\approx \frac{-\xi_0}{2\pi} \left[ \frac{2}{v_F} + \left( \frac{\xi_0^2}{v_F} + \frac{2\xi_0^4 \epsilon_F^2}{v_F^3} \right) \delta k_F^2 \right] \Delta^2 \log\left(\frac{D}{|\Delta|}\right).
\end{aligned}
\tag{3.36}
$$

The terms proportional to $\delta k_F$ are beyond our accuracy since

$$
\xi_0^2 J^2 \delta k_F^2 \sim \xi_0^2 \frac{J^2}{v_F^2} t_\perp^2 = \frac{\xi_0^2}{\xi_{EP}^2} t_\perp^2, \quad \xi_{EP} = \frac{v_F}{J}
\tag{3.37}
$$

which only yields a parametrically small contribution to the ground state energy and can thus be neglected. The resulting ground state energy is the same as for two uncoupled wires, in which one helicity is gapped per wire plus small corrections, which we neglect. The same procedure yields the same results for the combination $\theta_1 = \pi$, $\theta_2 = \pi$.

### 3.3.2. Normal metal phase

Let us now consider $\alpha_{\parallel 1} = \alpha_{\parallel 2} = 0$ and $\theta_1 = 0$, $\theta_2 = \pi$. In the picture of uncoupled chains we find, that the first quantum wire supports a helical phase with helicity $h1 = -1$ and the second wire a phase with helicity $h2 = +1$.
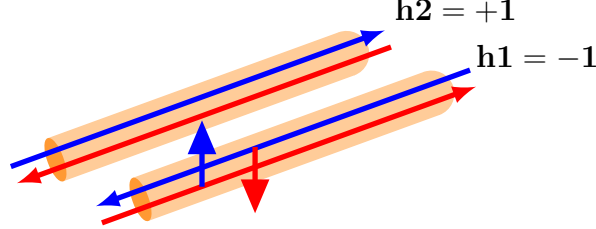


Figure 3.8: For this combination of angles, wire **1** and **2** have opposite helicities.

If we switch on the tunneling, electrons can now tunnel between the wires and move in every direction irrespective of their spin (including backscattering on the Kondo impurities). This is why we refer to this setup as normal metal phase, since it has an equal number of spins of the same type going left and right. However, it still needs to be checked, if the transport in this setup is protected or not. The Green's function is given by

$$
-\mathbf{G}_{0\pi}^{-1} = \left(\begin{array}{cccc|cccc}
\partial_{R_+} & \Delta_1 e^{i\delta k_F x} & 0 & \Delta_1 & 0 & 0 & 0 & 0 \\
\Delta_1^\dagger e^{-i\delta k_F x} & \partial_{L_+} & \Delta_1^\dagger & 0 & 0 & 0 & 0 & 0 \\
0 & \Delta_1 & \partial_{R_-} & \Delta_1 e^{-i\delta k_F x} & 0 & 0 & 0 & 0 \\
\Delta_1^\dagger & 0 & \Delta_1^\dagger e^{i\delta k_F x} & \partial_{L_-} & 0 & 0 & 0 & 0 \\
\hline
0 & 0 & 0 & 0 & \partial_{R_+} & \Delta_2 e^{i\delta k_F x} & 0 & -\Delta_2 \\
0 & 0 & 0 & 0 & \Delta_2^\dagger e^{-i\delta k_F x} & \partial_{L_+} & -\Delta_2^\dagger & 0 \\
0 & 0 & 0 & 0 & 0 & -\Delta_2 & \partial_{R_-} & \Delta_2 e^{-i\delta k_F x} \\
0 & 0 & 0 & 0 & -\Delta_2^\dagger & 0 & \Delta_2^\dagger e^{i\delta k_F x} & \partial_{L_-}
\end{array}\right)
\begin{array}{l}
R_{+\uparrow} \\ L_{+\downarrow} \\ R_{-\uparrow} \\ L_{-\downarrow} \\ R_{+\downarrow} \\ L_{+\uparrow} \\ R_{-\downarrow} \\ L_{-\uparrow}
\end{array}, \quad (3.38)
$$

where $\Delta_{1/2} = \mp\frac{\tilde{J}}{2} e^{-i\psi_{1/2}}$. In contrast to Eq. (3.24) we now have interband and intraband scattering between all fermions with the same helicity. We remove the oscillations from Eq. (3.38) with a gauge transformation on all fermions similar to Eq. (3.25). We can also gauge out the spin phases in $\Delta_{1/2}$, using a transformation similar to Eq. (3.32). We proceed by computing the ground state energy following the same steps which we used for the helical phase setup in Section 3.3.1. This gives

$$
\delta F_{0\pi} = \frac{-\xi_0}{2\pi} \left[ \frac{|\mathbf{\Delta}_1|^2}{v_{F_+}} + \frac{|\mathbf{\Delta}_1|^2}{v_{F_-}} + \frac{4|\mathbf{\Delta}_1|^2}{v_{F_+} + v_{F_-}} + 1 \leftrightarrow 2 \right] \Delta^2 \log\left(\frac{D}{|\Delta|}\right) =
$$
$$
= \frac{-\xi_0}{2\pi} \left[ \frac{(v_{F_+} + v_{F_-})^2 + 4 v_{F_-} v_{F_+}}{2 v_{F_-} v_{F_+}(v_{F_-} + v_{F_+})} \right] \Delta^2 \log\left(\frac{D}{|\Delta|}\right). \quad (3.39)
$$

In leading order of $\delta k_F$ we find for $\delta F_{\theta_1 \theta_2}$

$$\delta F_{0\pi} = \frac{-\xi_0}{2\pi} \left[ \frac{(v_{F_+} + v_{F_-})^2 + 4 v_{F_-} v_{F_+}}{2 v_{F_-} v_{F_+} (v_{F_-} + v_{F_+})} \right] \Delta^2 \log \left( \frac{D}{|\Delta|} \right) \approx$$

$$\approx \frac{-\xi_0}{2\pi} \left[ \frac{2}{v_F} + \left( \frac{\xi_0^2}{v_F} + \frac{\xi_0^4 \epsilon_F^2}{v_F^3} \right) \delta k_F^2 \right] \Delta^2 \log \left( \frac{D}{|\Delta|} \right), \quad (3.40)$$

which is slightly unfavoured compared to Eq. (3.36), but the difference between the ground state energies is beyond our accuracy. We thus recover again the ground state energy of two gapped sectors and two gapless sectors, which is in agreement with the fact, that at zero tunneling we have two wires with one gapped and one gapless mode each.

Our analysis of the ground state energy in the weak tunneling limit showed, that one cannot energetically distinguish (in our accuracy), which setup wins. A global helical setup, where both wires have the same helicity and normal metal setup, where both wires have the opposite helicity is equally likely to appear upon coupling of the chains. In the next section, we show how this degeneracy can be removed by considering a naturally present, intrinsic spin-orbit interaction.

## 3.4. Ground state energy degeneracy of two coupled wires

To remove the degeneracy between the two helical setups presented in the last section, we need to include a term, which biases the dispersion relation for different spins. In GaAs quantum wires there are two types of naturally present spin-orbit interactions. Let us consider a Dresselhaus spin-orbit interaction in the system of the form

$$\mathcal{H}_{SOI} = d\, c_{f,\sigma}^\dagger \left( -i \partial_x \right) \sigma_z^{\sigma\sigma'} c_{f,\sigma'}, \quad f = 1, 2. \quad (3.41)$$

The full Hamiltonian of the system is now given by Eq. (3.3) and $\mathcal{H}_{SOI}$. We assume a relatively weak SOI with a weak tunneling $t_\perp \ll d \ll J \ll D$. We diagonalize the Hamiltonian using the transformation

$$c_{\pm,\uparrow/\downarrow} = \frac{1}{\sqrt{2}} \left( c_{1\uparrow/\downarrow} \pm c_{2\uparrow/\downarrow} \right). \quad (3.42)$$

After switching to the Lagrangian description, the Lagrangian in the new basis reads as

$$\mathcal{L} = \sum_{\nu=\pm, \zeta=\uparrow/\downarrow} \left[ c_{\nu\zeta}^\dagger \, \varepsilon_{\nu\zeta} \, c_{\nu\zeta} + \frac{J_a}{2} \left( c_{\nu\zeta}^\dagger \, \mathbf{S}_{+a} \boldsymbol{\sigma}_a \, c_{\nu\zeta'} + c_{\nu\zeta}^\dagger \, \mathbf{S}_{-a} \boldsymbol{\sigma}_a \, c_{-\nu\zeta'} + h.c. \right) \right], \quad (3.43)$$

where $\mathbf{S}_\pm = \mathbf{S}_1 \pm \mathbf{S}_2$. Similar to Eq. (3.6) one finds intra- and interband scattering terms. The main difference is, that now, the dispersion for up and down spins is

shifted by an additional contribution $\pm dk$. The dispersion relation of the system including SOI, see Fig. 3.9, is given by

$$\varepsilon_{\pm\uparrow/\downarrow} = -2t\cos\left(k\xi_0\right) \mp t_\perp \pm dk,\tag{3.44}$$

For the position of the chemical potential in Fig. 3.9, we find four distinct pairs of Fermi points around which we linearize the dispersion. We introduce smooth chiral
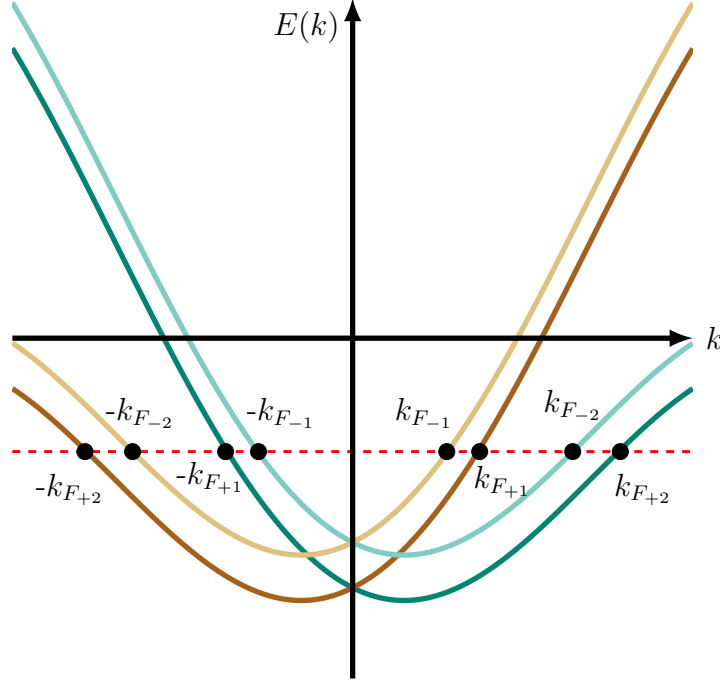


Figure 3.9: After taking into account the spin-orbit interaction we find eight Fermi points. The blue curves correspond to spin $\downarrow$ and the brown curves to spin $\uparrow$. In contrast to the splitting by tunneling here different helicities have distinct Fermi momenta and velocities.

fields in the following way

$$c_{\pm\uparrow} = e^{-ik_{F\pm1}x}\, R_{\pm\uparrow} + e^{ik_{F\pm2}x}\, L_{\pm\uparrow}\tag{3.45}$$

$$c_{\pm\downarrow} = e^{-ik_{F\pm2}x}\, R_{\pm\downarrow} + e^{ik_{F\pm1}x}\, L_{\pm\downarrow}\tag{3.46}$$

We insert Eqs. (3.45) and (3.46) in the Kondo interaction of Eq. (3.43) and select only the backscattering parts as before.

$$\mathcal{L} = \sum_{\nu=\pm}\left[ R^\dagger_{\nu\uparrow}\partial_{R\nu1}\, R_{\nu\uparrow} + L^\dagger_{\nu\downarrow}\partial_{L\nu1}\, L_{\nu\downarrow} + R^\dagger_{\nu\downarrow}\partial_{R\nu2}\, R_{\nu\downarrow} + L^\dagger_{\nu\uparrow}\partial_{L\nu2}\, L_{\nu\uparrow} + \right.$$
$$+ \frac{J_a}{2}\left( R^\dagger_{\nu\uparrow}\mathbf{S}_{+a}\boldsymbol{\sigma}_a L_{\nu\downarrow}\, e^{2ik_{F\nu1}x} + R^\dagger_{\nu\downarrow}\mathbf{S}_{+a}\boldsymbol{\sigma}_a L_{\nu\uparrow}\, e^{2ik_{F\nu2}x} \right.$$
$$\left.\left. + R^\dagger_{\nu\uparrow}\mathbf{S}_{-a}\boldsymbol{\sigma}_a L_{-\nu\downarrow}\, e^{i(k_{F\nu1}+k_{F-\nu1})x} + R^\dagger_{\nu\downarrow}\mathbf{S}_{-a}\boldsymbol{\sigma}_a L_{-\nu\uparrow}\, e^{i(k_{F\nu2}+k_{F-\nu2})x} + h.c.\right)\right],\tag{3.47}$$

where $\partial_{R/L\nu1/2} = \partial_\tau \mp iv_{F\nu\zeta}\partial_x \pm d$ is the chiral derivative with the Fermi velocity $v_{F\pm1/2} = 2t\xi_0\sin\left(k_{F\pm1/2}\xi_0\right)$ corresponding to the respective bands. Note, that the

intraband scattering $\sim \mathbf{S}_+$ oscillates with either $k_{F_\nu 1}$ or $k_{F_\nu 2}$. The interband scattering $\sim \mathbf{S}_-$ oscillates with either $k_{F_\nu 1} + k_{F_{-\nu} 1}$ or $k_{F_\nu 2} + k_{F_{-\nu} 2}$. Not all oscillations can be absorbed in to the spins and there will be residual oscillations.

We assume that the spin-orbit interaction is large compared to the tunneling and we expect a scale separation. This means, that $k_{F_\nu 1} \ll k_{F_\nu 2}$, but $k_{F_\nu 1} \approx k_{F_{-\nu} 1}$ and $k_{F_\nu 2} \approx k_{F_{-\nu} 2}$, are of the same magnitude. Without a loss of generality, we parameterize the spin $\mathbf{S}_+$ to absorb the respective oscillations corresponding to $k_{F_{-2}} \lesssim \tilde{k}_{F_2} \lesssim k_{F_{+2}}$, with the mean $\tilde{k}_{F_{1/2}} = \frac{1}{2}\left(k_{F_{+1/2}} + k_{F_{-1/2}}\right)$ and the difference $\delta k_{F_{1/2}} = k_{F_{+1/2}} - k_{F_{-1/2}}$.

$$
\frac{\mathbf{S}_\pm}{s} = \mathbf{m}_1 \pm \mathbf{m}_2 + \left[\mathbf{e}_1^{(1)}\sqrt{1-\mathbf{m}_1^2} \pm \mathbf{e}_1^{(2)}\sqrt{1-\mathbf{m}_2^2}\right]\cos\left(2\tilde{k}_{F_2}x\right) +
$$
$$
+ \left[\mathbf{e}_2^{(1)}\sqrt{1-\mathbf{m}_1^2} \pm \mathbf{e}_2^{(2)}\sqrt{1-\mathbf{m}_2^2}\right]\sin\left(2\tilde{k}_{F_2}x\right), \quad (3.48)
$$

Inserting the spherical basis vectors Eqs. (2.7)–(2.9) and selecting only the non-oscillating parts, we find the backscattering Lagrangian to be of a similar form like Eqs. (3.17)–(3.20)

$$
\mathcal{L}_{BS}^{\pm\pm(h1)} = \mathrm{R}_{\pm\uparrow}^\dagger \left[\Delta_+^{(h1)}\right] \mathrm{L}_{\pm\downarrow}\, e^{2i\left(k_{F_{\pm 1}}-\tilde{k}_{F_2}\right)x} + h.c., \quad (3.49)
$$

$$
\mathcal{L}_{BS}^{\pm\pm(h2)} = \mathrm{R}_{\pm\downarrow}^\dagger \left[\Delta_+^{(h2)}\right] \mathrm{L}_{\pm\uparrow}\, e^{\pm i\delta k_{F_2}x} + h.c., \quad (3.50)
$$

$$
\mathcal{L}_{BS}^{\pm\mp(h1)} = \mathrm{R}_{\pm\uparrow}^\dagger \left[\Delta_-^{(h1)}\right] \mathrm{L}_{\mp\downarrow}\, e^{2i\left(\tilde{k}_{F_1}-\tilde{k}_{F_2}\right)x} + h.c., \quad (3.51)
$$

$$
\mathcal{L}_{BS}^{\pm\mp(h2)} = \mathrm{R}_{\pm\downarrow}^\dagger \left[\Delta_-^{(h2)}\right] \mathrm{L}_{\mp\uparrow} + h.c., \quad (3.52)
$$

where $\Delta_\pm^{(h1/h2)}$ is defined in Eqs. (3.21) and (3.22). We now use the fact that $k_{F_\nu 1}$ and $k_{F_\nu 2}$ are of different magnitude. This means, that the difference between the Fermi momenta $k_{F_\nu 1}$ and $k_{F_\nu 2}$ is large. Equations (3.49) and (3.51) are still fast oscillating terms and we neglect them. Note, that one obtains backscattering terms only for fermions $\mathrm{R}_{\nu\downarrow}, \mathrm{L}_{\nu\uparrow}$, which have helicity $h = -1$. We could have also chosen to absorb Fermi momenta close to $\tilde{k}_{F_1}$ into the spin configuration in Eq. (3.48). In this case we would neglect the scattering terms Eqs. (3.50) and (3.52) instead of Eqs. (3.49) and (3.51), leaving only backscattering terms for the helicity $h = +1$. We proceed by analyzing the helical phase setup with spin-orbit interaction.

### 3.4.1. The helical phase with spin–orbit interaction

We chose to absorb momenta close to $\tilde{k}_{F_2}$. Let us now again consider $\alpha_{\parallel 1} = \alpha_{\parallel 2} = 0$. The fermionic gaps in Eqs. (3.50) and (3.52) are maximal for $\theta_1 = \pi$, $\theta_2 = \pi$. This means, that spin orbit favored gapping the helicity $h = -1$. This leaves us with gapless modes of helicity $h = +1$.

The corresponding Green's function including tunneling and spin–orbit interaction is given by

$$
\mathbf{-G}_{00}^{-1} = \left(\begin{array}{cccc|cccc}
\partial_{R_{+\uparrow}} & 0 & 0 & 0 & 0 & 0 & 0 & 0 \\
0 & \partial_{L_{+\downarrow}} & 0 & 0 & 0 & 0 & 0 & 0 \\
0 & 0 & \partial_{R_{-\uparrow}} & 0 & 0 & 0 & 0 & 0 \\
0 & 0 & 0 & \partial_{L_{-\downarrow}} & 0 & 0 & 0 & 0 \\
\hline
0 & 0 & 0 & 0 & \partial_{R_{+\downarrow}} & \Delta_+ e^{i\delta k_{F_2}x} & 0 & \Delta_- \\
0 & 0 & 0 & 0 & \Delta_+^\dagger e^{-i\delta k_{F_2}x} & \partial_{L_{+\uparrow}} & \Delta_-^\dagger & 0 \\
0 & 0 & 0 & 0 & 0 & \Delta_- & \partial_{R_{-\downarrow}} & \Delta_+ e^{-i\delta k_{F_2}} \\
0 & 0 & 0 & 0 & \Delta_-^\dagger & 0 & \Delta_+^\dagger e^{i\delta k_{F_2}x} & \partial_{L_{-\uparrow}}
\end{array}\right)
\begin{array}{l}
R_{+\uparrow} \\ L_{+\downarrow} \\ R_{-\uparrow} \\ L_{-\downarrow} \\ R_{+\downarrow} \\ L_{+\uparrow} \\ R_{-\downarrow} \\ L_{-\uparrow}
\end{array}, \quad (3.53)
$$

where $\Delta_\pm = -\frac{\Delta}{2}\left(e^{-i\psi_1} \pm e^{-i\psi_2}\right)$ and the ordering of the states is indicated to the right. We remove the oscillations in the lower right block of Eq. (3.53) by a gauge transformation similar to Eq. (3.25). We also gauge out the spin phases using Eq. (3.32). The ground state energy of the system can be computed similarly to before. The constant shift $\pm d$ in the chiral derivatives does not enter the ground state energy equation. Furthermore, we neglect the splitting caused by the tunneling, since we already showed, that it only has a negligible influence. This gives the following ground state energy

$$
\delta F_{\pi\pi}^{\tilde{k}_{F_2}} \approx \frac{-\xi_0}{\pi v_{F_2}} \Delta^2 \log\left(\frac{D}{|\Delta|}\right), \tag{3.54}
$$

where $v_{F_2} = 2t\xi_0 \sin\left(\tilde{k}_{F_2}\xi_0\right)$, the superscript denotes the absorbed Fermi momentum and the subscript denotes our choice of angles $\theta_1$ and $\theta_2$. If we absorb Fermi momenta close to $k_{F_{\pm 1}}$ instead, we find through exactly the same procedure the ground state energy

$$
\delta F_{00}^{\tilde{k}_{F_1}} \approx \frac{-\xi_0}{\pi v_{F_1}} \Delta^2 \log\left(\frac{D}{|\Delta|}\right). \tag{3.55}
$$

If we assume, that $0 < \tilde{k}_{F_1} \ll \tilde{k}_{F_2} < \frac{\pi}{2\xi_0}$, then the Fermi velocity $v_{F_{1/2}} = 2t\xi_0 \sin\left(k_{F_{1/2}}\xi_0\right)$ is a monotonously increasing function of the Fermi momentum.

$$
v_{F_1} < v_{F_2} \rightarrow |\delta F_{00}^{\tilde{k}_{F_2}}| < \delta|F_{00}^{\tilde{k}_{F_1}}|, \tag{3.56}
$$

As a consequence, the absorption of momenta close to $\tilde{k}_{F_1}$ and hence a spin configuration which gaps all fermions with helicity $h = +1$ is favored over a spin configuration, which gaps all fermions with helicity $h = -1$.

### 3.4.2. The normal metal phase with spin–orbit interaction

Let us consider $\alpha_{\|1} = \alpha_{\|2} = 0$ and $\theta_1 = 0$, $\theta_2 = \pi$. The corresponding Green's function including tunneling and spin–orbit interaction is given by

$$
\mathbf{-G}_{0\pi}^{-1} = \left(\begin{array}{cccc:cccc}
\partial_{R_{+\uparrow}} & 0 & 0 & 0 & 0 & 0 & 0 & 0 \\
0 & \partial_{L_{+\downarrow}} & 0 & 0 & 0 & 0 & 0 & 0 \\
0 & 0 & \partial_{R_{-\uparrow}} & 0 & 0 & 0 & 0 & 0 \\
0 & 0 & 0 & \partial_{L_{-\downarrow}} & 0 & 0 & 0 & 0 \\
\hdashline
0 & 0 & 0 & 0 & \partial_{R_{+\downarrow}} & \Delta_2 e^{i\delta k_{F_2}x} & 0 & -\Delta_2 \\
0 & 0 & 0 & 0 & \Delta_2^\dagger e^{-i\delta k_{F_2}x} & \partial_{L_{+\uparrow}} & -\Delta_2^\dagger & 0 \\
0 & 0 & 0 & 0 & 0 & -\Delta_2 & \partial_{R_{-\downarrow}} & \Delta_2 e^{-i\delta k_{F_2}x} \\
0 & 0 & 0 & 0 & -\Delta_2^\dagger & 0 & \Delta_2^\dagger e^{i\delta k_{F_2}x} & \partial_{L_{-\uparrow}}
\end{array}\right)
\begin{array}{l}
R_{+\uparrow} \\ L_{+\downarrow} \\ R_{-\uparrow} \\ L_{-\downarrow} \\ R_{+\downarrow} \\ L_{+\uparrow} \\ R_{-\downarrow} \\ L_{-\uparrow}
\end{array}, \quad (3.57)
$$

We follow the same steps as for the helical phase setup. We again neglect the splitting caused by the tunneling. This gives the following ground state energy for absorbed momenta close to $\tilde{k}_{F_1}$ or $\tilde{k}_{F_2}$

$$
\delta F_{0\pi}^{\tilde{k}_{F_1}} \approx \frac{-\xi_0}{2\pi v_{F_1}} \Delta^2 \log\left(\frac{D}{|\Delta|}\right). \tag{3.58}
$$

$$
\delta F_{0\pi}^{\tilde{k}_{F_2}} \approx \frac{-\xi_0}{2\pi v_{F_2}} \Delta^2 \log\left(\frac{D}{|\Delta|}\right). \tag{3.59}
$$

We again assume, that $0 < \tilde{k}_{F_1} \ll \tilde{k}_{F_2} < \frac{\pi}{2\xi_0}$ and find, that the configuration in which momenta close to $\tilde{k}_{F_{\pm 1}}$ are absorbed is favored.

$$
v_{F_1} < v_{F_2} \rightarrow |\delta F_{00}^{\tilde{k}_{F2}}| < |\delta F_{00}^{\tilde{k}_{F1}}|, \tag{3.60}
$$

If we compare Eqs. (3.55) and (3.58) we can see, that the spin-orbit interaction favors the setup, where $\theta_1 = 0$ and $\theta_2 = 0$ or $\theta_1 = \pi$ and $\theta_2 = \pi$, respectively.

$$
|\delta F_{0\pi}^{\tilde{k}_{F1}}| = \frac{1}{2}|\delta F_{00}^{\tilde{k}_{F1}}|. \tag{3.61}
$$

This means, that in the presence of spin-orbit interaction a global helical phase can emerge, where one helicity is favored energetically. For our choice of parameters, the gapless modes have helicity $h = -1$. To favor the other helicity one has to flip the sign of the spin-orbit interaction $d \leftrightarrow -d$.

## 3.5. Collective modes, transport and disorder

### 3.5.1. Helical phase

Let us consider the case where $\alpha_{\|1} = \alpha_{\|2} = 0$ and $\theta_1 = 0$, $\theta_2 = 0$. Equation (3.24) is the corresponding Green's function of this setup. The spectrum of the gapped block at $\delta\psi = 0$ is given by

$$\varepsilon(k) = \pm\sqrt{+\frac{1}{2}k^2\left(v_{F_-}^2 + v_{F_+}^2\right) + \Delta^2 \pm \frac{1}{2}\sqrt{k^4\left(v_{F_-}^2 - v_{F_+}^2\right)^2}}. \qquad (3.62)$$

All four fermions $R_{+\uparrow}, L_{+\downarrow}, R_{-\uparrow}, L_{-\downarrow}$ are gapped with a gap of $\mathcal{O}(\Delta)$. After integrating out the gapped fermions, one finds the following action for the remaining gapless modes.

$$\mathcal{L} = \frac{\delta F_{00}}{\xi_0} + \mathcal{L}_0[R_\downarrow, L_\uparrow] + \mathcal{L}_{LL}[\tilde{\psi}, v_F] + \mathcal{L}_{WZ}^{(sl)}, \qquad (3.63)$$

where the ungapped action now is supplemented by the ground state energy equation of the gapped fermions. The term $\mathcal{L}_{LL}[\tilde{\psi}, v_F]$ is the chiral anomaly, see Eq. (C.22), which appears after the gauge transformation in Eq. (3.32). The Luttinger liquid Lagrangian is the quantum analog of a classical hydrodynamic Lagrangian and is characterized through a compressibility $K_\psi$ and velocity $v_\psi$. In Refs. [1–4] it was demonstrated, that integrating out the remaining massive fields in Eq. (3.63) leads to a strong renormalization of the velocity and Luttinger parameter $K_\psi \ll 1$. The field $\tilde{\psi}$ is a collective helical mode, because it couples to external charge and spin sources simultaneously. The remaining gapless helical fermions can be bosonized and form a helical Luttinger liquid. The low energy excitations are thus given by

$$\mathcal{L} = \mathcal{L}_{LL}[\Phi^{(h2)}, v_F] + \mathcal{L}_{LL}[\tilde{\psi}, v_\psi], \quad K_\Phi = 1, \quad K_\psi << 1. \qquad (3.64)$$

The transport properties of these helical Luttinger liquids are similar to those of the one dimensional Kondo chain. If one adds spinless disorder to each wire individually one finds

$$\mathcal{L}_{\mathrm{dis}} = g(x)\, R_{1\sigma}^\dagger L_{1\sigma} + h.c. + 1 \leftrightarrow 2. \qquad (3.65)$$

It is easy to show, that the transformation into the $\pm$ basis does not mix the disorders and one obtains disorder for each band individually

$$\mathcal{L}_{\mathrm{dis}} = g(x)\, R_{+\sigma}^\dagger L_{+\sigma} + h.c. + + \leftrightarrow -. \qquad (3.66)$$

Disorder does not scatter between the channels. Integrating out the gapped variables similar to Section 2.2.4 thus gives the same parametrical suppresion of backscattering effects for the gapless fermions $R_{+\downarrow}, L_{+\uparrow}, R_{-\downarrow}, L_{-\uparrow}$.

### 3.5.2. Normal metal phase

For the normal metal phase we chose the angles $\alpha_{\|1} = \alpha_{\|2} = 0$ and $\theta_1 = 0, \theta_2 = \pi$. The corresponding Green's function is given by Eq. (3.38). The spectrum of one gapped block is given by

$$\varepsilon(k) = \pm\sqrt{\frac{1}{2}\left(k^2\left(v_{F_-}^2 + v_{F_+}^2 + \Delta^2\right) \pm \tilde{\Delta}(k)\right)}, \qquad (3.67)$$

where $\tilde{\Delta}(k) = \sqrt{\Delta^4 + k^4\left(v_{F_-}^2 - v_{F_+}^2\right)^2 + \Delta^2 k^2(v_{F_-} - v_{F_+})^2}$. In the normal metal phase two fermions are gapped with a gap of $\mathcal{O}(\Delta)$ and two fermions possess a
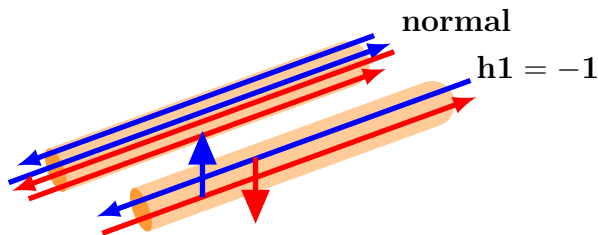
Figure 3.10: Spin-orbit interaction effectively removes one helical gap. This leads to a normal quantum wire, in which spins can move in both directions and a helical quantum wire coupled via tunneling.

parametrically small gap. Switching on spin orbit interaction removes the helical gap from one of the wires. In the previous chapter, the helicity $h = +1$ remains gapped. This effectively gives us one normal mode and one helical mode with a parametrically small gap, which we can neglect, because it turns out, that it is beyond our accuracy. The low energy Lagrangian after integrating out all gapped fermions and massive fields is given by

$$\mathcal{L} = \mathcal{L}_{LL}[\Phi^{(h2)}, v_F] + \mathcal{L}_{LL}[\tilde{\psi}_1, v_{\psi 1}], \tag{3.68}$$

where the field $\Phi^{(h2)}$ describes the gapless helical fermions $\mathrm{R}_{\pm\downarrow}, \mathrm{L}_{\pm\uparrow}$. The field $\psi_1$ is a collective helical excitation stemming from the gauge transformation on the remaining gapped helical mode. Its Fermi velocity and compressibility is again strongly renormalized $K_{\psi_1} \ll 1$. Adding spinless disorder now leads to a completely different situation, since helical fermions can now tunnel at any point and time into the normal mode. This effectively removes the protection of the transport in the normal metal setup.

## 3.6. The Isotropic Kondo chain

The previous approach can be extended to a fully isotropic Kondo chain, where we do not distinguish the interaction strengths in different directions of the chains $J_x = J_y = J_z = J$. The Lagrangian of two isotropic, coupled chains in the diagonalized basis is given by

$$\mathcal{L} = \sum_{a,\nu=\pm} \left[ \mathrm{R}_\nu^\dagger \partial_{R_\nu} \mathrm{R}_\nu + \mathrm{L}_\nu^\dagger \partial_{L_\nu} \mathrm{L}_\nu + \right.$$
$$\left. + \frac{J}{2} \left( \mathrm{R}_\nu^\dagger \mathbf{S}_+ \cdot \boldsymbol{\sigma} \, \mathrm{L}_\nu \, e^{2ik_{F_\nu}x} + \mathrm{R}_\nu^\dagger \mathbf{S}_- \cdot \boldsymbol{\sigma} \, \mathrm{L}_{-\nu} \, e^{i(k_{F_+}+k_{F_-})x} + h.c. \right) \right]. \tag{3.69}$$

We can insert the parameterization for the spins given by Eq. (3.14) and express the basis vectors through SU(2) matrices, see Appendix E.

$$\mathbf{e}_{1,2,3} = \frac{1}{2} \left[ \boldsymbol{\sigma} g \sigma_{x,y,z} g^{-1} \right], \tag{3.70}$$

where $g$ is a smooth function of $x$ and $\tau$. It is convenient to work in a rotated basis.

$$\tilde{R} = g^{-1}R, \quad \tilde{L} = g^{-1}L \qquad (3.71)$$

"Helical" fermions in the rotated basis now consist of linear combinations of up and down spins. Slow spin fluctuations restore the broken SU(2) symmetry. This has severe consequences, as one for example looses the applicability as a spin filter. The authors of Refs. [2,3] have derived a fully quantum mechanical theory and showed its stability.

The semiclassical analysis of the sections Section 3.3 can be performed in a similar fashion for the isotropic Kondo chain. First one finds the classical spin configurations, which minimizes the free energy. We integrate out all fermionic and spin degree of freedom whose fluctiations are gapped. The remaining fluctuating spin degrees of freedom can be treated fully quantum mechanically. This approach is justified by the seperation of energy scales, since one assumes, that the length scale set by $k_F^{-1}$ is much smaller than the coherence length of gapped variables $\xi = v_F/J$. We thus expect the same qualitative behavior for two coupled anisotropic Kondochains and isotropic Kondochains regarding the presence of a quasi-one dimensional helical phase.

## 3.7. Strongly coupled chains $J_K \ll 2t \ll t_\perp$

Let us analyze the quasi-one-dimensional Kondo chain in the strong tunneling limit $J_K \ll 2t \ll t_\perp$, see Fig. 3.3(c). For concreteness, we place the chemical potential in the lower band. The upper band fermions are well seperated by a large gap. The only possible interband scattering processes are thus (classically forbidden) virtual tunneling processes. To account for the virtual processes we perturbatively integrate out the upper band fermions. We start from Eq. (3.6)

$$\mathcal{L} = \sum_{a,\nu=\pm} \left[ c_\nu^\dagger \, \varepsilon_\nu \, c_\nu + \frac{J_a}{2} \left( c_\nu^\dagger \, \mathbf{S}_{+a} \boldsymbol{\sigma}_a \, c_\nu + c_\nu^\dagger \, \mathbf{S}_a \boldsymbol{\sigma}_a \, c_{-\nu} + h.c. \right) \right], \qquad (3.72)$$

We define the Green's function of the upper and lower band as $-\mathbf{G}_\pm^{-1}$, with

$$-\mathbf{G}_+^{-1}(\tau, x) = \partial_\tau + \varepsilon_0 - \varepsilon_F - \mu + \frac{J_a}{2} \mathcal{M}_+^a \qquad (3.73)$$

$$-\mathbf{G}_-^{-1}(\tau, x) = \partial_\tau + \varepsilon_0 - \varepsilon_F + 2t_\perp + \frac{J_a}{2} \mathcal{M}_+^a, \qquad (3.74)$$

where $\mathcal{M}_+^a$ is a matrix containing all the backscattering amplitudes defined by Eqs. (3.17)–(3.20). Next, we integrate out the fermions in the upper $(-)$ band. We

use the identity

$$
\left\langle \exp\left(\int d\tau\, dx \left\{ \frac{J_a}{2} \left[ c_+^\dagger \left( \mathbf{S}_- \cdot \boldsymbol{\sigma} \right)^a c_- + h.c. \right] \right\} \right) \right\rangle_- =
$$
$$
= \exp\left( \frac{J_a J_b}{8} \int dM \left\{ \left[ c_+^\dagger \left( \boldsymbol{\sigma} \cdot \mathbf{S}_- \right)^a \right]_{\tau_1, x_1} \left[ \langle c_-^\dagger c_- \rangle_- \right]_{\substack{\tau_1 - \tau_2, \\ x_1 - x_2}} \left[ \left( \mathbf{S}_- \cdot \boldsymbol{\sigma} \right)^b c_+ \right]_{\tau_2, x_2} \right\} \right),
$$
$$(3.75)$$

where $M = \{\tau_1, \tau_2, x_1, x_2\}$. To proceed we expand the Green's function of the upper band in leading order of $\frac{J}{t_\perp}$. This gives

$$
J_a J_b \mathbf{G}_- = \frac{J_a J_b}{\partial_\tau + \varepsilon_0 - \varepsilon_F + 2t_\perp} \frac{1}{1 + \frac{J_c \boldsymbol{\mathcal{M}}_+^c}{\partial_\tau + \varepsilon_0 - \varepsilon_F + 2t_\perp}} \approx \frac{J_a J_b}{2t_\perp} + \mathcal{O}\left( \frac{J_a J_b}{t_\perp^2}, \dots \right), \quad (3.76)
$$

where we used a symbolic inversion denoted by the fractions in Eq. (3.76). Equation (3.75) is a self energy contribution for the fermions in the lower (+) band. Inserting Eq. (3.76) in Eq. (3.75) we find

$$
\exp\left( \frac{J_a J_b}{16 t_\perp} \int d\tau\, dx \left\{ c_+^\dagger \left( \boldsymbol{\sigma} \cdot \mathbf{S}_- \right)^a \left( \mathbf{S}_- \cdot \boldsymbol{\sigma} \right)^b c_+ \right\} \right) =
$$
$$
= \exp\left( \frac{J_a J_b}{16 t_\perp} \int d\tau\, dx \left\{ c_+^\dagger \left[ \mathbf{S}_-^2\, \sigma_0\, \delta_{a,b} + \underbrace{i\,\varepsilon_{abc}\, \mathbf{S}_-^a \mathbf{S}_-^b \sigma_c}_{=\mathbf{S}_-(\tau) \times \mathbf{S}_-(\tau) = 0} \right] c_+ \right\} \right). \quad (3.77)
$$

Hence, the action for the lower band in leading order of $\frac{1}{t_\perp}$ is given by

$$
S = \int d\tau\, dx \left\{ c_+^\dagger \left[ -\mathbf{G}_+^{-1} - \frac{J_a^2}{16 t_\perp} \left( \mathbf{S}_-^2 \right)^a \sigma_0 \right] c_+ \right\}. \quad (3.78)
$$

The additional term $\sim \mathbf{S}_-^2$ is a parametrically small contribution to the action of the lower band Green's function. It becomes more relevant for spins larger than $s > 4\sqrt{t_\perp/J}$, but we consider spins which must statisfy $sJ \ll 2t$. Hence, it is subleading and beyond our accuracy. We thus obtain an effective one band model, which can be treated similar to Refs. [1–4] and is able to support helical transport.

# 4

# Summary & Outlook

In this work we studied a quasi-one dimensional magnetically doped quantum wire and analyzed its transport properties. The theoretical model consists of two one dimensional Kondo chains, which are dense and coupled via an interchain hopping term.

First, we discussed a simple setup consisting of two itinerant electron systems coupled to a single impurity chain. After the formation of the impurity spin helix, the fermionic sector, with either helicity $h = +1$ or $h = -1$, will be gapped in both wires. This results in a helical phase.

Next, we focused on a non-trivial setup consisting of two weakly coupled Kondo chains. We considered an interchain hopping, which is much smaller than the gap produced by the Kondo interaction. In this case, there is a degeneracy of the ground state of the system, in which either both wires host fermions with the same helicity or both wires host fermions of opposite helicity . Besides the gapless fermions one finds a small number of helical fermions residing slightly above and below the gap. These fermions have a strongly renormalized Fermi velocity.

We suggest that a Dresselhaus type spin-orbit interaction can remove the aforementioned degeneracy. Dresselhaus spin-orbit interaction is naturally present in many materials, which are used to produce quantum wires, such as GaAs. We analyzed the regime, where the energy scale set by the interchain tunneling is much smaller than the energy scale of the spin-orbit interaction. Both are weak compared to the Kondo interaction. Depending on the sign of the spin-orbit interaction one will always find a helical phase with helicity $h = +1$ or $h = -1$ supported by compound fermions in both channels.

Finally, we analyzed the opposing regime of strongly coupled chains. Treating the inverse tunneling strength perturbatively, one recovers an effective one band model, for which the transport properties, such as protected helical transport and the emergence of slow collective helical modes are known [1, 4].

We believe that the intermediate tunneling regime, where the tunneling is of the same order as the gap produced by the Kondo interaction, can be analyzed in a similar way. However, there is no perturbative solution for this problem. Instead

one has to fully take into account the back scattering processes generated by the Kondo interaction. It is still an open question, whether the results obtained in this thesis remain qualitatively valid if one considers other tunneling geometries or an odd number of Kondo chains. The authors of Ref. [1] have shown that for finite temperatures, the broken helicity is restored due to thermal fluctuations. The thermal fluctuations lead to domain walls, where the helicity of the Kondo chain changes. It is an open question how quasi-one dimensional Kondo chains behave at finite temperatures.

Hence we predict a possibility for helical transport in the limit of weak and strong tunneling in quasi-one dimensional magnetically doped quantum wires. Our work can give a push to start the realization of helical states in quasi-one dimensional geometries.

# Bibliography

[1] A. M. Tsvelik and O. M. Yevtushenko. Quantum Phase Transition and Protected Ideal Transport in a Kondo Chain. *Phys. Rev. Lett.*, **115**, 21 216402. (2015).

[2] A. M. Tsvelik and O. M. Yevtushenko. Physics of arbitrarily doped Kondo lattices: From a commensurate insulator to a heavy Luttinger liquid and a protected helical metal. *Phys. Rev. B*, **100**, 16 165110. (2019).

[3] A. Tsvelik and O. Yevtushenko. Helicity-protected Transport in Magnetically Doped One-Dimensional Wires. *preprint*, **arXiv:1902.01787**. (2019).

[4] D. Schimmel et al. Low energy properties of the Kondo chain in the RKKY regime. *New J. Phys.*, **18**, 053004. (2016).

[5] A. P. Schnyder, S. Ryu, A. Furusaki, and A. W. W. Ludwig. Classification of topological insulators and superconductors in three spatial dimensions. *Phys. Rev. B*, **78**, 19 195125. (2008).

[6] A. Altland and M. R. Zirnbauer. Nonstandard symmetry classes in mesoscopic normal-superconducting hybrid structures. *Phys. Rev. B*, **55**, 2 1142–1161. (1997).

[7] K. von Klitzing. The quantized Hall effect. *Rev. Mod. Phys.*, **58**, 3 519–531. (1986).

[8] D. J. Thouless, M. Kohmoto, M. P. Nightingale, and M. den Nijs. Quantized Hall Conductance in a Two-Dimensional Periodic Potential. *Phys. Rev. Lett.*, **49**, 6 405–408. (1982).

[9] R. B. Laughlin. Quantized Hall conductivity in two dimensions. *Phys. Rev. B*, **23**, 10 5632–5633. (1981).

[10] F. D. M. Haldane. Model for a Quantum Hall Effect without Landau Levels: Condensed-Matter Realization of the "Parity Anomaly". *Phys. Rev. Lett.*, **61**, 18 2015–2018. (1988).

[11] C. L. Kane and E. J. Mele. $\mathbb{Z}_2$ Topological Order and the Quantum Spin Hall Effect. *Phys. Rev. Lett.*, **95**, 14 146802. (2005).

[12] C. L. Kane and E. J. Mele. Quantum Spin Hall Effect in Graphene. *Phys. Rev. Lett.*, **95**, 22 226801. (2005).

[13] B. A. Bernevig and S.-C. Zhang. Quantum Spin Hall Effect. *Phys. Rev. Lett.*, **96**, 10 106802. (2006).

[14] M. König, S. Wiedmann, C. Brüne, A. Roth, H. Buhmann, L. W. Molenkamp, X.-L. Qi, and S.-C. Zhang. Quantum Spin Hall Insulator State in HgTe Quantum Wells. *Science*, **318**, 5851 766–770. (2007).

[15] M. König, H. Buhmann, L. W. Molenkamp, T. Hughes, C.-X. Liu, X.-L. Qi, and S.-C. Zhang. The Quantum Spin Hall Effect: Theory and Experiment. *Journal of the Physical Society of Japan*, **77**, 3 031007. (2008).

[16] C. H. L. Quay, T. L. Hughes, J. A. Sulpizio, L. N. Pfeiffer, K. W. Baldwin, K. W. West, D. Goldhaber-Gordon, and R. de Picciotto. Observation of a one-dimensional spin-orbit gap in a quantum wire. *Nature Physics*, **6**, 5 336–339. (2010).

[17] S. Heedt, N. Traverso Ziani, F. Crépin, W. Prost, S. Trellenkamp, J. Schubert, D. Grützmacher, B. Trauzettel, and T. Schäpers. Signatures of interaction-induced helical gaps in nanowire quantum point contacts. *Nature Physics*, **13** 563–567. (2017).

[18] J. Kammhuber, M. C. Cassidy, F. Pei, M. P. Nowak, A. Vuik, Ö. Gül, D. Car, S. R. Plissard, E. P. A. M. Bakkers, M. Wimmer, and L. P. Kouwenhoven. Conductance through a helical state in an Indium antimonide nanowire. *Nature Communications*, **8**, 1 478. (2017).

[19] N. Kainaris and S. T. Carr. Emergent topological properties in interacting one-dimensional systems with spin-orbit coupling. *Phys. Rev. B*, **92**, 3 035139. (2015).

[20] B. Braunecker, P. Simon, and D. Loss. Nuclear magnetism and electron order in interacting one-dimensional conductors. *Phys. Rev. B*, **80**, 16 165119. (2009).

[21] J. Klinovaja, G. J. Ferreira, and D. Loss. Helical states in curved bilayer graphene. *Phys. Rev. B*, **86**, 23 235416. (2012).

[22] J. Klinovaja, M. J. Schmidt, B. Braunecker, and D. Loss. Helical Modes in Carbon Nanotubes Generated by Strong Electric Fields. *Phys. Rev. Lett.*, **106**, 15 156809. (2011).

[23] B. Braunecker, P. Simon, and D. Loss. Nuclear Magnetism and Electronic Order in $^{13}$C Nanotubes. *Phys. Rev. Lett.*, **102**, 11 116403. (2009).

[24] C. P. Scheller, T.-M. Liu, G. Barak, A. Yacoby, L. N. Pfeiffer, K. W. West, and D. M. Zumbühl. Possible Evidence for Helical Nuclear Spin Order in GaAs Quantum Wires. *Phys. Rev. Lett.*, **112**, 6 066801. (2014).

[25] M. Rümmeli, M. Löffler, C. Kramberger, F. Simon, F. Fulop, O. Jost, R. Schönfelder, A. Grüneis, T. Gemming, W. Pompe, B. Büchner, and T. Pichler. Isotope-Engineered Single-Wall Carbon Nanotubes; A Key Material for Magnetic Studies. *Journal of Physical Chemistry C*, **111**. (2007).

[26] F. Simon, C. Kramberger, R. Pfeiffer, H. Kuzmany, V. Zólyomi, J. Kürti, P. M. Singer, and H. Alloul. Isotope Engineering of Carbon Nanotube Systems. *Phys. Rev. Lett.*, **95**, 1 017401. (2005).

[27] H. O. H. Churchill, A. J. Bestwick, J. W. Harlow, F. Kuemmeth, D. Marcos, C. H. Stwertka, S. K. Watson, and C. M. Marcus. Electron-nuclear interaction in $^{13}$C nanotube double quantum dots. *Nature Physics*, **5**, 5 321–326. (2009).

[28] B. Jäck, Y. Xie, J. Li, S. Jeon, B. A. Bernevig, and A. Yazdani. Observation of a Majorana zero mode in a topologically protected edge channel. *Science*, **364**, 6447 1255–1259. (2019).

[29] J. Rincón, A. Moreo, G. Alvarez, and E. Dagotto. Exotic Magnetic Order in the Orbital-Selective Mott Regime of Multiorbital Systems. *Phys. Rev. Lett.*, **112**, 10 106405. (2014).

[30] Y. Nambu, K. Ohgushi, S. Suzuki, F. Du, M. Avdeev, Y. Uwatoko, K. Munakata, H. Fukazawa, S. Chi, Y. Ueda, and T. J. Sato. Block magnetism coupled with local distortion in the iron-based spin-ladder compound $BaFe_2Se_3$. *Phys. Rev. B*, **85**, 6 064413. (2012).

[31] L. Riegger, N. Darkwah Oppong, M. Höfer, D. R. Fernandes, I. Bloch, and S. Fölling. Localized Magnetic Moments with Tunable Spin Exchange in a Gas of Ultracold Fermions. *Phys. Rev. Lett.*, **120**, 14 143601. (2018).

[32] M. Kanász-Nagy, Y. Ashida, T. Shi, C. P. Moca, T. N. Ikeda, S. Fölling, J. I. Cirac, G. Zaránd, and E. A. Demler. Exploring the anisotropic Kondo model in and out of equilibrium with alkaline-earth atoms. *Phys. Rev. B*, **97**, 15 155156. (2018).

[33] H. Tsunetsugu, M. Sigrist, and K. Ueda. The ground-state phase diagram of the one-dimensional Kondo lattice model. *Rev. Mod. Phys.*, **69**, 3 809–864. (1997).

[34] G. Honner and M. Gulácsi. One-Dimensional Kondo Lattice at Partial Band Filling. *Phys. Rev. Lett.*, **78**, 11 2180–2183. (1997).

[35] E. Novais, E. Miranda, A. H. Castro Neto, and G. G. Cabrera. Coulomb gas approach to the anisotropic one-dimensional Kondo lattice model at arbitrary filling. *Phys. Rev. B*, **66**, 17 174409. (2002).

[36] O. Zachar, S. A. Kivelson, and V. J. Emery. Exact Results for a 1D Kondo Lattice from Bosonization. *Phys. Rev. Lett.*, **77**, 7 1342–1345. (1996).

[37] M. Troyer and D. Würtz. Ferromagnetism of the one-dimensional Kondo-lattice model: A quantum Monte Carlo study. *Phys. Rev. B*, **47**, 5 2886–2889. (1993).

[38] Khait Ilia, Azaria Patrick, Hubig Claudius, Schollwöck Ulrich, and Auerbach Assa. Doped Kondo chain, a heavy Luttinger liquid. *Proceedings of the National Academy of Sciences of the United States of America*, **115**, 20 5140–5144. (2018).

[39] A. M. Tsvelik. Semiclassical solution of one dimensional model of Kondo insulator. *Phys. Rev. Lett.*, **72**, 7 1048–1051. (1994).

[40] E. Novais, E. Miranda, A. H. Castro Neto, and G. G. Cabrera. Phase Diagram of the Anisotropic Kondo Chain. *Phys. Rev. Lett.*, **88**, 21 217201. (2002).

[41] J. C. Xavier and E. Miranda. Correlation exponent $K_\rho$ of the one-dimensional Kondo lattice model. *Phys. Rev. B*, **70**, 7 075110. (2004).

[42] N. Shibata and K. Ueda. The one-dimensional Kondo lattice model studied by the density matrix renormalization group method . *Journal of Physics: Condensed Matter*, **11**, 2. (1999).

[43] J. Maciejko. Kondo lattice on the edge of a two-dimensional topological insulator. *Phys. Rev. B*, **85**, 24 245108. (2012).

[44] B. L. Altshuler, I. L. Aleiner, and V. I. Yudson. Localization at the Edge of a 2D Topological Insulator by Kondo Impurities with Random Anisotropies. *Phys. Rev. Lett.*, **111**, 8 086401. (2013).

[45] O. Yevtushenko, A. Wugalter, V. I. Yudson, and B. L. Altshuler. Transport in helical Luttinger liquid with Kondo impurities. *EPL*, **112**, 5. (2015).

[46] V. Yudson and O. Yevtushenko. Protection of helical transport in Quantum Spin Hall samples: the role of symmetries on edges. *preprint*, **arXiv:1909.08460**. (2019).

[47] H. Tsunetsugu, M. Sigrist, and K. Ueda. The ground-state phase diagram of the one-dimensional Kondo lattice model. *Rev. Mod. Phys.*, **69**, 3 809–864. (1997).

[48] P. Coleman. *Heavy Fermions: Electrons at the Edge of Magnetism.* American Cancer Society, 2007.

[49] Doniach S. The Kondo lattice and weak antiferromagnetism. *Physica B+C*, **91** 231–234. (1977).

[50] T. Giamarchi. *Quantum Physics in One Dimension.* Clarendon Press, (2004).

[51] A. Tsvelik. *Quantum Field Theory in Condensed Matter Physics* . Cambridge: Cambridge University Press, (2003).

# A Appendix A
# Linearizing the dispersion of the KC

## A.1. Fourier Transformation of the tight-binding Hamiltionian

We use the following convention for Fourier Transformation:

$$c_{j,\sigma} = \frac{1}{\sqrt{L}} \sum_k c_{k,\sigma}\, e^{-ik\mathbf{R}_j}, \tag{A.1}$$

$$c_{j,\sigma}^\dagger = \frac{1}{\sqrt{L}} \sum_k c_{k,\sigma}^\dagger\, e^{ik\mathbf{R}_j}, \tag{A.2}$$

where $L$ denotes the system size, $\mathbf{R}_j$ denotes a reciprocal lattice vector. We insert the transformations in the tight-binding Hamiltonian and find

$$
\begin{aligned}
\mathcal{H}_0 &= -t\left(c_{j+1,\sigma}^\dagger\, c_{j,\sigma} + h.c.\right) = -\frac{t}{L}\left(c_{k,\sigma}^\dagger\, c_{p,\sigma}\, e^{jk\mathbf{R}_{j+1}} e^{-jp\mathbf{R}_j} + h.c.\right) = \\
&= -\frac{t}{L}\left(c_{k,\sigma}^\dagger\, c_{p,\sigma}\, e^{j(k-p)\mathbf{R}_j} e^{jk\xi_0} + h.c.\right) = -\frac{t}{L}\left(c_{k,\sigma}^\dagger\, c_{p,\sigma}\, L\delta_{k,p} e^{jk\xi_0} + h.c.\right) = \\
&= -t\left(c_{k,\sigma}^\dagger\, c_{k,\sigma}\, e^{jk\xi_0} + h.c.\right) = \underbrace{-2t\cos(k\xi_0)}_{\varepsilon(k)}\, c_{k,\sigma}^\dagger\, c_{k,\sigma}, \quad (\mathrm{A.3})
\end{aligned}
$$

where $\xi_0$ is the lattice constant of our chain.

## A.2. Linearization procedure for the 1D Kondochain

It is convenient to project the fermionic operators on the low energy sector by linearizing the dispersion relation and introducing new smooth chiral operators. This works best if we are far away from the band edges. We assume $|J_K| < |\mu| \ll t$ and use the last expression of Eq. (A.3) as a starting point and introduce a chemical potential $\mathcal{H}_\mu = -\mu\, c_k^\dagger\, c_k$.

$$\mathcal{H}_0 \approx \sum_{k=k_F-\Lambda}^{k_F+\Lambda} (\varepsilon(k) - \mu)\, c_{k,\sigma}^\dagger\, c_{k,\sigma} + \sum_{k=-k_F-\Lambda}^{-k_F+\Lambda} (\varepsilon(k) - \mu)\, c_{k,\sigma}^\dagger\, c_{k,\sigma}, \tag{A.4}$$
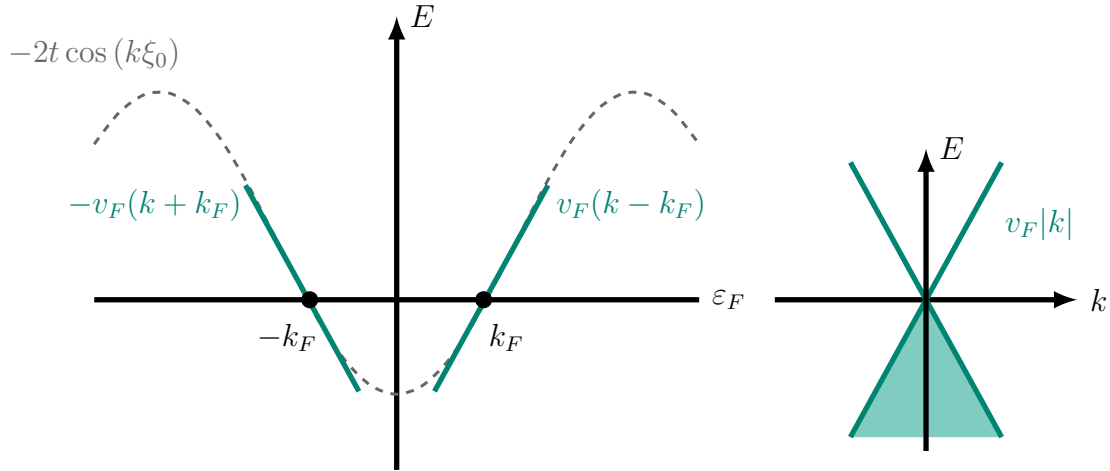
Figure A.1: Linearization procedure for the tight-binding Hamiltonian. Since we are only interested in the low energy behavior of our system close to the Fermi surface, we can approximate the dispersion relation as linear. This approximation is valid if the density of states is constant around the Fermi surface i.e. if we are far away from the band edges. It is convenient to define chiral operators $R, L$ by shifting the original fermion operators.

where $\Lambda$ is a momentum cut-off, which satisfies $|k| < \Lambda$. Since we only care about low lying excitations, it is a valid approximation to extend $\Lambda \to \infty$.

We shift the first sum to $k - k_F \to k$ and the second sum to $k + k_F \to k$ and introduce smooth right and left moving fields

$$\text{R}_{k,\sigma} = \text{c}_{k+k_F,\sigma}, \quad \text{L}_{k,\sigma} = \text{c}_{k-k_F,\sigma}. \tag{A.5}$$

We linearize $\varepsilon(k)$ around the respective Fermi points $\pm k_F$ to linear order in the momentum. This gives

$$\varepsilon(k)|_{k \approx k_F} \approx \varepsilon_F + v_F(k - k_F) \tag{A.6}$$

$$\varepsilon(k)|_{k \approx -k_F} \approx \varepsilon_F - v_F(k + k_F), \tag{A.7}$$

where $\varepsilon_F = -2t \cos(k_F \xi_0)$ and $v_F = 2t\xi_0 \sin(k_F \xi_0)$.

We can express the original fermion field operator in position space through the new smooth modes in the following way.

$$\text{c}_{j,\sigma} = \frac{1}{\sqrt{L}} \sum_k \text{c}_{k,\sigma}\, e^{ikn\xi_0} =$$

$$= \frac{1}{\sqrt{L}} \left[ \sum_{k=k_F-\Lambda}^{k_F+\Lambda} \text{c}_{k,\sigma}\, e^{ikn\xi_0} + \sum_{k=-k_F-\Lambda}^{-k_F+\Lambda} \text{c}_{k,\sigma}\, e^{ikn\xi_0} \right] \approx$$

$$\approx \frac{1}{\sqrt{L}} \left[ e^{-ik_F n\xi_0} \sum_k \text{R}_{k,\sigma}\, e^{ikn\xi_0} + e^{ik_F n\xi_0} \sum_k \text{L}_{k,\sigma}\, e^{ikn\xi_0} \right] =$$

$$= e^{-ik_F x} \text{R}_\sigma(x) + e^{ik_F x} \text{L}_\sigma(x), \quad \text{(A.8)}$$

where we defined

$$R_\sigma(x) = \frac{1}{\sqrt{L}} \sum_k R_\sigma e^{ikn\xi_0}, \tag{A.9}$$

$$L_\sigma(x) = \frac{1}{\sqrt{L}} \sum_k L_\sigma e^{ikn\xi_0}. \tag{A.10}$$

We insert the last line of Eq. (A.8) in Eq. (2.1) and keep only the non-oscillatory terms for $\mathcal{H}_0$. The oscillating terms in the backscattering part of $\mathcal{H}_{KI}$ can be absorbed in the spin configuration. After taking the continuum limit of the sums in position space we find for the Lagrangian density

$$\mathcal{L}_0 = R_\sigma^\dagger \, \partial_R \, R_\sigma + L_\sigma^\dagger \, \partial_L \, L_\sigma, \quad \partial_{R/L} = \partial_\tau \mp i v_F \partial_x \tag{A.11}$$

where $\tau_0, \tau_z$ are Pauli matrices, which act in the chiral space. For the Kondo interaction

$$\mathcal{H}_{KI} = \sum_a J^a \, c_{m,\sigma}^\dagger \, \mathbf{S}_m^a \cdot \boldsymbol{\sigma}_a^{\sigma\sigma'} \, c_{m,\sigma'}, \tag{A.12}$$

we find a forward scattering and backscattering contribution.

$$\mathcal{L}_{FS} = \rho_s J_a \, R_\sigma^\dagger \, \mathbf{S}^a \cdot \boldsymbol{\sigma}_a^{\sigma\sigma'} \, R_{\sigma'} + R \leftrightarrow L, \tag{A.13}$$

$$\mathcal{L}_{BS} = \rho_s J_a \, R_\sigma^\dagger \, \mathbf{S}^a \cdot \boldsymbol{\sigma}_a^{\sigma\sigma'} \, L_{\sigma'} \, e^{2ik_F x} + h.c. \tag{A.14}$$

where we expressed the sum over the impurity spin positions as an integral times a constant spin density $\rho_s$: $\sum_{j \in M} \to \frac{\rho_s}{\xi_0} \int dx$ and rescaled $R, L \to \sqrt{\xi_0} \, R, L$.

$$\mathcal{L}_\perp = \sum_{j,\sigma} \left( -t_\perp \, c_{j,1}^\dagger \, c_{j,2} + h.c. \right), \tag{A.15}$$

gives

$$\mathcal{L}_\perp = \sum_\sigma -t_\perp \, R_{1,\sigma}^\dagger \, R_{2,\sigma} + L_{1,\sigma}^\dagger \, L_{2,\sigma} + h.c. \tag{A.16}$$

We proceed in a similar way with the hopping Hamiltonian

$$\mathcal{H}_\perp = -t_\perp \sum_i c_{i,\sigma,1}^\dagger \, c_{i,\sigma,2} + h.c. = -\frac{t_\perp}{N} \sum_{i,\sigma,k,p} c_{k,\sigma,1}^\dagger \, c_{p,\sigma,2} \, e^{i(k-p)\mathbf{R}_i} + h.c. =$$

$$= -t_\perp \sum_{k,\sigma} c_{k,\sigma,1}^\dagger \, c_{k,\sigma,2} + h.c. \tag{A.17}$$

## A.3. Diagonalization

The full Hamiltonian, without the RKKY-interaction can therfore be written as

$$\mathcal{H}_{full}\big|_{\Delta=0} = \sum_{k,\sigma} \begin{pmatrix} c^{\dagger}_{k,\sigma,1} \\ c^{\dagger}_{k,\sigma,2} \end{pmatrix} \begin{pmatrix} \varepsilon(k) & -t_{\perp} \\ -t_{\perp} & \varepsilon(k) \end{pmatrix} \begin{pmatrix} c_{k,\sigma,1} \\ c_{k,\sigma,2} \end{pmatrix}. \tag{A.18}$$

We want to diagonalize this matrix and find the form of the RKKY-interaction, after applying the unitary transformation which diagonalizes the Hamiltonian. The eigenvalues of the Hamiltonian are given by

$$(\varepsilon(k) - E_{\pm})^2 - t_{\perp}^2 \overset{!}{=} 0 \Leftrightarrow E_{\pm} = \varepsilon(k) \pm t_{\perp}. \tag{A.19}$$

The Eigenvectors can be found from

$$\begin{pmatrix} -t_{\perp} & -t_{\perp} \\ -t_{\perp} & -t_{\perp} \end{pmatrix} v_{+} \overset{!}{=} 0 \Leftrightarrow v_{+} = \frac{1}{\sqrt{2}} \begin{pmatrix} 1 \\ -1 \end{pmatrix}, \tag{A.20}$$

$$\begin{pmatrix} t_{\perp} & -t_{\perp} \\ -t_{\perp} & t_{\perp} \end{pmatrix} v_{-} \overset{!}{=} 0 \Leftrightarrow v_{-} = \frac{1}{\sqrt{2}} \begin{pmatrix} 1 \\ 1 \end{pmatrix}. \tag{A.21}$$

We define our similarity transformation in the following way $U = \{v_{-}, v_{+}\}$. We note that $U = U^T = U^{-1}$. This gives us the following Hamiltonian

$$\mathcal{H}_{full}\big|_{\Delta=0} = \sum_{k,\sigma} \begin{pmatrix} \psi^{\dagger}_{k,\sigma,+} \\ \psi^{\dagger}_{k,\sigma,-} \end{pmatrix} \begin{pmatrix} \varepsilon(k) - t_{\perp} & 0 \\ 0 & \varepsilon(k) + t_{\perp} \end{pmatrix} \begin{pmatrix} \psi_{k,\sigma,+} \\ \psi_{k,\sigma,-} \end{pmatrix}, \tag{A.22}$$

where we introduced a new spinor defined via

$$\psi_k = \begin{pmatrix} \psi_{k,\sigma,+} \\ \psi_{k,\sigma,-} \end{pmatrix} = \frac{1}{\sqrt{2}} \begin{pmatrix} 1 & 1 \\ 1 & -1 \end{pmatrix} \begin{pmatrix} c_{k,\sigma,1} \\ c_{k,\sigma,2} \end{pmatrix} = \frac{1}{\sqrt{2}} \begin{pmatrix} c_{k,\sigma,1} + c_{k,\sigma,2} \\ c_{k,\sigma,1} - c_{k,\sigma,2} \end{pmatrix}. \tag{A.23}$$

We refer to $\psi_{(-)+}$ as (anti-)symmetric combination of operators.

# B

## Appendix B

# Ground state energy of gapped 1D Dirac fermions

## B.1. Groundstate energy of gapped fermions

Let us consider a gapped fermionic Green's function of the form

$$-\mathbf{G}^{-1} = \begin{pmatrix} -i\omega + v_{F_1}k & \Delta \\ \Delta & -i\omega - v_{F_2}k \end{pmatrix} = -\mathbf{G}_0^{-1} + \mathbf{\Delta}, \tag{B.1}$$

where

$$-\mathbf{G}_0^{-1} = \begin{pmatrix} -i\omega + v_{F_1}k & 0 \\ 0 & -i\omega - v_{F_2}k \end{pmatrix}, \quad \mathbf{\Delta} = \begin{pmatrix} 0 & \Delta \\ \Delta & 0 \end{pmatrix}. \tag{B.2}$$

The partition function corresponding to Eq. (B.1) is given by

$$Z = \det\left(-\mathbf{G}^{-1}\right) = \det\left(-\mathbf{G}_0^{-1} + \mathbf{\Delta}\right) = Z_0 \exp \operatorname{Tr} \log\left(1 - \mathbf{G}_0\mathbf{\Delta}\right), \tag{B.3}$$

where we used that $\det\left(\mathbf{A}\right) = \exp \operatorname{Tr} \log\left(\mathbf{A}\right)$ in the last step. From the partition function we compute the free energy $F = -T \log\left(Z\right)$, and expand the free energy in leading order of $\Delta$. We find

$$F = F_0 - T \operatorname{Tr} \log\left(1 - \mathbf{G}_0\mathbf{\Delta}\right) \approx F_0 + \frac{T}{2} \operatorname{Tr} \mathbf{G}_0\mathbf{\Delta}\mathbf{G}_0\mathbf{\Delta}. \tag{B.4}$$

Note that the linear term in the expansion is absent, because of the off diagonal structure of $\mathbf{\Delta}$ and on the other hand reflects the fact, that we expand the ground state energy around its minimum. In the limit $T \to 0$ we can convert the summation over the Matsubara frequency to an integral and find

$$\delta F = \frac{T}{2} \operatorname{Tr} \mathbf{G}_0\mathbf{\Delta}\mathbf{G}_0\mathbf{\Delta} \to -\xi_0 \int \frac{d\{\omega, k\}}{(2\pi)^2} \frac{\Delta^2}{(-i\omega + v_{F_1}k)(-i\omega - v_{F_2}k)}, \tag{B.5}$$

which has poles at $\omega = \mp i v_{F_{1/2}}k$. We find

$$\delta F = -\frac{\xi_0}{\pi} \int_\Delta^D dk \frac{\Delta^2}{k\left(v_{F_1} + v_{F_2}\right)} = -\frac{\xi_0}{\pi\left(v_{F_1} + v_{F_2}\right)} \Delta^2 \log\left(\frac{D}{\Delta}\right), \tag{B.6}$$

where we used the band width as a high energy cut-off.

## B.2. Groundstate energy of gapped fermions with an oscillating gap

Consider a Green's function of the form

$$-\mathbf{G}^{-1} = \begin{pmatrix} -i\omega + v_F k & \Delta e^{-i\delta k_F x} \\ \Delta e^{i\delta k_F x} & -i\omega - v_F k \end{pmatrix}, \tag{B.7}$$

We use a gauge transformation to remove the oscillations

$$\mathrm{R} \to \mathrm{R}\, e^{-\frac{i\delta k_F x}{2}}, \quad \mathrm{L} \to \mathrm{L}\, e^{\frac{i\delta k_F x}{2}}, \tag{B.8}$$

which gives a constant shift in the chemical potential, reading as

$$-\mathbf{G}^{-1} = \begin{pmatrix} -i\omega + v_F k & \Delta \\ \Delta & -i\omega - v_F k \end{pmatrix} - \frac{v_F \delta k_F}{2}. \tag{B.9}$$

# C

## Appendix C

# Bosonization identities

## C.1. General identities

### C.1.1. Bosonization of fermions with four degrees of freedom

The basics of Bosonization and a complete introduction can be found in Giamarchis book [50]. Here we only summarize the parts which are important for our calculations here. We define $(\mathrm{R}\,/\,\mathrm{L})_{\uparrow,\downarrow} \equiv \Phi_{(\mathrm{R}\,/\,\mathrm{L}),\uparrow,\downarrow}$ and start from the bosonization identity

$$\Phi_{r,s} = \frac{1}{\sqrt{2\pi\xi_0}} \hat{U}_s e^{-\frac{i}{\sqrt{2}}[r\phi_c - \theta_c + sr\phi_s - s\theta_s]}, \tag{C.1}$$

where $r = \pm 1$ for R/L fields and $s = \pm 1$ for $\uparrow, \downarrow$. Similar to [50] we define

$$\phi_{c,s} = \frac{1}{\sqrt{2}} \left[ \phi_\uparrow \pm \phi_\downarrow \right], \tag{C.2}$$

and a similar relation for the $\theta$ field. We evaluate the density of the fields using the point splitting technique

$$\Phi_{r,s}^\dagger(x)\Phi_{r,s}(x) = \lim_{\xi_0 \to 0} \left[ \Phi_{r,s}^\dagger(x + \xi_0)\Phi_{r,s}(x) \right] \tag{C.3}$$

to account for the lattice nature of the Hamiltionian. We use the Baker-Campbell-Hausdorff formula $e^X e^Y = e^{X+Y} e^{[X,Y]/2}$ to evaluate the product. The commutator of the boson fields can be reduced to

$$\left[ \frac{i}{\sqrt{2}} \left( r\phi_c' - \theta_c' + sr\phi_s' - s\theta_s' \right), -\frac{i}{\sqrt{2}} \left( r\phi_c - \theta_c + sr\phi_s - s\theta_s \right) \right] = \tag{C.4}$$

$$= +\frac{i\pi r}{4} \underbrace{\left( (1+s)^2 + (1-s)^2 \right)}_{2(1+s^2)=4}, \tag{C.5}$$

where $'$ denotes the dependence on $x + \xi_0$ and we used that the commutator is given by $[\phi_j(x'), \theta_j(x)] = \frac{i\pi}{2} \operatorname{sign}(x - x')$ with $j = \uparrow, \downarrow$. All other commutators vanish. This means that BCH gives an additional $e^{ir\frac{\pi}{2}} = ir$. This gives

$$\Phi_{r,s}^\dagger(x)\Phi_{r,s}(x) = \frac{-r}{2\pi\sqrt{2}} \left[ r\nabla\phi_c - \nabla\theta_c + sr\nabla\phi_s - s\nabla\theta_s \right] \tag{C.6}$$

$$\Phi_{r,s}^{\dagger}(x)(i\partial_x)\Phi_{r,s}(x) = \frac{-r}{4\pi}\left[r\nabla\phi_c - \nabla\theta_c + sr\nabla\phi_s - s\nabla\theta_s\right]^2 \tag{C.7}$$

$$\Phi_{r,s}^{\dagger}(x)(\partial_\tau)\Phi_{r,s}(x) = \frac{ir}{4\pi}\left[r\nabla\phi_c - \nabla\theta_c + sr\nabla\phi_s - s\nabla\theta_s\right]\left[\nabla \leftrightarrow \partial\tau\right] \tag{C.8}$$

For the free electron Lagrangian we find that

$$\mathcal{L}_e = \sum_{r=\pm1,s=\uparrow,\downarrow} \Phi_{r,s}^{\dagger}(\partial_\tau - rv_F i\partial_x)\Phi_{r,s} = \mathcal{L}_{LL,dual}[\phi_c,\theta_c] + \mathcal{L}_{LL,dual}[\phi_s,\theta_s], \tag{C.9}$$

where

$$\mathcal{L}_{LL,dual}[\phi,\theta] = -\frac{i}{\pi}\partial_\tau\phi\nabla\theta + \frac{v_F}{2\pi}\left[\nabla\phi^2 + \nabla\theta^2\right]. \tag{C.10}$$

Equation (C.10) can be obtained by inserting Eqs. (C.6)–(C.8), after integrating the imaginary time derivative by parts and rescaling of fields by $\phi,\theta \to \frac{1}{\sqrt{2}}(\phi,\theta)$ .

### C.1.2. Bosonization of fermions with eight degrees of freedom

Coupling the wires will double our number of d.o.f. Following the notations of Giamarchi, we introduce new bosonic fields which are linear combinations of the bosonic fields of the two coupled wires.

$$\phi_{c,s}^{\pm} = \frac{1}{\sqrt{2}}\left[\phi_{c,s}^1 \pm \phi_{c,s}^2\right], \tag{C.11}$$

where $c, s$ stand for the charge and spin sector of the bosonic fields. We treat the new orbital index $f = 1,2$ formally as a spin-1/2 variable. This leads to the following representation for the fermionic fields.

$$\Psi_{r,s,f} = \frac{1}{\sqrt{2\pi\xi_0}}\hat{U}_{r,s,f}e^{(-i/2)\left[r\phi_c^+ - \theta_c^+ + f\left(r\phi_c^- - \theta_c^-\right) + s\left(r\phi_s^+ - \theta_s^+ + f\left(r\phi_s^- - \theta_s^-\right)\right)\right]}, \tag{C.12}$$

where we again defined $(\mathrm{R}\,/\,\mathrm{L})_{(\uparrow,\downarrow),(1,2)} \equiv \Psi_{(\mathrm{R}\,/\,\mathrm{L}),(\uparrow,\downarrow),(1,2)}$. When used in a mathematical expression $f = \pm1$ stands for the first and second wire, $s = \pm1$ stands for $\uparrow,\downarrow$ in the wire and $r = \pm1$ stands for right- and leftmoving fermions. For the derivation of equation (C.15) we use the point-splitting technique to account for the lattice nature of our Hamiltonian:

$$\Psi_{r,s,f}^{\dagger}(x)\Psi_{r,s,f}(x) = \lim_{\xi_0 \to 0}\left[\Psi_{r,s,f}^{\dagger}(x + \xi_0)\Psi_{r,s,f}(x)\right], \tag{C.13}$$

and the Baker-Campbell-Hausdorff formula $e^X e^Y = e^{X+Y}e^{[X,Y]/2}$. The commutator of the boson fields can be reduced to

$$\frac{1}{8}\left[r\phi_c'^+ - \theta_c'^+ + f\left(r\phi_c'^- - \theta_c'^-\right) + s\left(r\phi_s'^+ - \theta_s'^+ + f\left(r\phi_s'^- - \theta_s'^-\right)\right), x' \leftrightarrow x\right] =$$
$$-\frac{r}{2}\underbrace{[\phi',\theta]}_{-\frac{i\pi}{2}}\underbrace{\left(1 + s^2 + f^2 + (fs)^2\right)}_{=4} = i\pi r, \tag{C.14}$$

where the primed fields indicate the dependence of the variable $x' = x + \xi_0$. This gives again an additional factor of $e^{ir\frac{\pi}{2}} = ir$ according to the BCH formula.

We now calculate the fermionic bilinears for equal $f, s, r$

$$
\Psi^\dagger_{r,s,f}\Psi_{r,s,f} = \frac{-r}{4\pi}\left[r\nabla\phi^+_c - \nabla\theta^+_c + fr\nabla\phi^-_c - f\nabla\theta^-_c + \right.
$$
$$
\left. + sr\nabla\phi^+_s - s\nabla\theta^+_s + fsr\nabla\phi^-_s - fs\nabla\theta^-_s\right], \quad \text{(C.15)}
$$

$$
\Psi^\dagger_{r,s,f}(i\partial x)\Psi_{r,s,f} = \frac{-r}{8\pi}\left[r\nabla\phi^+_c - \nabla\theta^+_c + fr\nabla\phi^-_c - f\nabla\theta^-_c + \right.
$$
$$
\left. + sr\nabla\phi^+_s - s\nabla\theta^+_s + fsr\nabla\phi^-_s - fs\nabla\theta^-_s\right]^2, \quad \text{(C.16)}
$$

$$
\Psi^\dagger_{r,s,f}(\partial_\tau)\Psi_{r,s,f} = \frac{ir}{8\pi}\left[r\nabla\phi^+_c - \nabla\theta^+_c + fr\nabla\phi^-_c - f\nabla\theta^-_c + \right.
$$
$$
\left. + sr\nabla\phi^+_s - s\nabla\theta^+_s + fsr\nabla\phi^-_s - fs\nabla\theta^-_s\right][\nabla \leftrightarrow \partial_\tau], \quad \text{(C.17)}
$$

and arbitrary $f, s, r$, respectively:

$$
\Psi^\dagger_{r,s,f}\Psi_{r',s',f'} =
$$
$$
= \frac{1}{2\pi\xi_0}\hat{U}^\dagger_{r,s,f}\hat{U}_{r,s,f}exp[(+i/2)[(r-r')\phi^+_c + (fr - f'r')\phi^-_c - (f - f')\theta^-_c + 
$$
$$
+ (sr - s'r')\phi^+_s - (s - s')\theta^+_s + (fsr - f's'r')\phi^-_s - (fs - f's')\theta^-_s]] \quad \text{(C.18)}
$$

Like before we want can bosonize the free Lagrangian given by

$$
\mathcal{L}_e = \sum_{r=\pm1, s=\uparrow,\downarrow, f=\pm1}\Psi^\dagger_{r,s,f}(\partial_\tau - rv_F i\partial_x)\Psi_{r,s,f} = \sum_{a=\pm, b=c,s}\mathcal{L}_{LL,dual}[\phi^a_b, \theta^a_b], \quad \text{(C.19)}
$$

where

$$
\mathcal{L}_{LL,dual}[\phi, \theta] = -\frac{i}{\pi}\partial_\tau\phi\nabla\theta + \frac{v_F}{2\pi}\left[\nabla\phi^2 + \nabla\theta^2\right], \quad \text{(C.20)}
$$

which can be again obtained after integration by parts and rescaling.

Often it is convenient to average over the dual fields in the following sense $\langle e^{ca}\rangle_a = e^{\frac{c^2}{2}\langle aa\rangle}$. When averaging over the linear term, we get the prefactor squared times the covariance of the field divided by 2. This can be shown by completing the square in the action. If we average $\mathcal{L}_{LL,dual}[\phi, \theta]$ over $\theta$ we get

$$
Z = \int \mathcal{D}\phi\,\mathcal{D}\theta\,e^{-\int d\tau dx\,\mathcal{L}_{LL,dual}[\phi,\theta]} = \mathcal{D}\phi\,e^{-\int d\tau dx\frac{1}{2\pi v_F}\left[(v_F\nabla\phi)^2 + (\partial_\tau\phi)^2\right]}, \quad \text{(C.21)}
$$

where we got a new expression for the Luttinger liquid, which is only described by the field $\phi$

$$
\mathcal{L}_{LL}[\phi, v_F] = \frac{1}{2\pi v_F}\left[(v_F\nabla\phi)^2 + (\partial_\tau\phi)^2\right] \quad \text{(C.22)}
$$

## C.2. Bosonization and phaseshift of relevant expressions

The fermionic part of the Lagrangian for two coupled wires reads

$$\mathcal{L} = \sum_f \left( \mathcal{L}_{e,f} + \mathcal{L}_{bs,f}^{sl} \right) + \mathcal{L}_\perp, \tag{C.23}$$

where

$$\mathcal{L}_\perp = t_\perp \left( R_1^\dagger\, R_2 + L_1^\dagger\, L_2 + h.c. \right), \tag{C.24}$$

$$\mathcal{L}_{e,f} = R_f^\dagger\, \partial_+\, R_f + L_f^\dagger\, \partial_-\, L_f, \quad \partial_\pm = \partial_\tau \mp i v_F \partial_x, \tag{C.25}$$

$$\mathcal{L}_{BS}^{sl} \sim e^{i\psi - i\alpha}\, R_f^\dagger\, \sigma_-\, L_f + e^{-i\psi - i\alpha}\, R_f^\dagger\, \sigma_+\, L_f + e^{-i\alpha}\, R_f^\dagger\, \sigma_z\, L_f + h.c. \tag{C.26}$$

All important fermionic bilinears for the backscattering term are

$$R_f^\dagger\, \sigma_z\, L_f = \frac{1}{2\pi\xi_0} e^{i\sqrt{2}\phi_c^f} \big( e^{i\sqrt{2}\phi_s^f} - e^{-i\sqrt{2}\phi_s^f} \big), \tag{C.27}$$

$$R_f^\dagger\, \sigma_+\, L_f = \frac{1}{2\pi\xi_0} e^{i\sqrt{2}(\phi_c^f - \theta_s^f)}, \tag{C.28}$$

$$L_f^\dagger\, \sigma_+\, R_f = \frac{1}{2\pi\xi_0} e^{i\sqrt{2}(-\phi_c^f - \theta_s^f)}, \tag{C.29}$$

$$L_f^\dagger\, \sigma_-\, R_f = \frac{1}{2\pi\xi_0} e^{i\sqrt{2}(-\phi_c^f + \theta_s^f)}, \tag{C.30}$$

$$R_f^\dagger\, \sigma_-\, L_f = \frac{1}{2\pi\xi_0} e^{i\sqrt{2}(+\phi_c^f + \theta_s^f)}. \tag{C.31}$$

All important fermionic bilinears for the tunneling term are

$$R_{1\uparrow}^\dagger\, R_{2\uparrow} = \frac{1}{2\pi\xi_0} e^{i(\phi_c^- - \theta_c^- + \phi_s^- - \theta_s^-)}, \tag{C.32}$$

$$R_{1\downarrow}^\dagger\, R_{2\downarrow} = \frac{1}{2\pi\xi_0} e^{i(\phi_c^- - \theta_c^- - \phi_s^- + \theta_s^-)}, \tag{C.33}$$

$$L_{1\uparrow}^\dagger\, L_{2\uparrow} = \frac{1}{2\pi\xi_0} e^{i(-\phi_c^- - \theta_c^- - \phi_s^- - \theta_s^-)}, \tag{C.34}$$

$$L_{1\downarrow}^\dagger\, L_{2\downarrow} = \frac{1}{2\pi\xi_0} e^{i(-\phi_c^- - \theta_c^- + \phi_s^- + \theta_s^-)}, \tag{C.35}$$

$$+ h.c. \tag{C.36}$$

# D

# Derivation of the slow Wess-Zumino action

We derive the Wess-Zumino action which naturally occurs in a path integral approach to spins. We will follow the derivation of [51]. We represent a spin with the usual Schwinger boson representation given by

$$S_i^a = \frac{1}{2} \, b_{i,\sigma}^\dagger \, \sigma_a^{\sigma,\sigma'} \, b_{i,\sigma'}, \quad a = x, y, z, \tag{D.1}$$

where $\sigma_a$ are Pauli matrices in the spin space $\{\uparrow, \downarrow\}$. We want the spins to satisfy the spin algebra $[S^a, S^b] = iS^c \varepsilon_{abc}$ and the relation $S^2 = s(s+1)$ for a spin of magnitude $s$. The algebra can be shown by simple insertion:

$$
\begin{aligned}
[S_i^a, S_j^b] &= \frac{1}{4} \left( b_{i,\alpha}^\dagger \, b_{i,\beta} \, b_{j,\gamma}^\dagger \, b_{j,\delta} - b_{j,\gamma}^\dagger \, b_{j,\delta} \, b_{i,\alpha}^\dagger \, b_{i,\beta} \right) \sigma_a^{\alpha,\beta} \sigma_b^{\gamma,\delta} = \\
&= \frac{1}{4} \left( b_{i,\alpha}^\dagger \, b_{j,\delta} \, \delta_{\beta,\gamma} - b_{j,\gamma}^\dagger \, b_{i,\beta} \, \delta_{\alpha,\delta} \right) \sigma_a^{\alpha,\beta} \sigma_b^{\gamma,\delta} \delta_{i,j} = \frac{1}{4} \delta_{i,j} \underbrace{\left( \sigma_a^{\sigma,\beta} \sigma_b^{\beta,\sigma'} - \sigma_b^{\sigma',\alpha} \sigma_a^{\alpha,\sigma} \right)}_{[\sigma_a,\sigma_b] = 2i\varepsilon_{abc}\sigma_c} b_{i,\sigma}^\dagger \, b_{i,\sigma'} = \\
&\hspace{9cm} = \delta_{i,j} i\varepsilon_{abc} S_i^c. \tag{D.2}
\end{aligned}
$$

The second requirement however sets a constraint onto the boson operators.

$$
\begin{aligned}
s(s+1) = S^2 = S_i^x S_i^x + S_i^y S_i^y + S_i^z S_i^z &= \frac{1}{2} \left( S_i^+ S_i^- + S_i^- S_i^+ \right) + S_i^z S_i^z = \\
&= \frac{1}{2} \left( b_{i,\uparrow}^\dagger \, b_{i,\downarrow} \, b_{i,\downarrow}^\dagger \, b_{i,\uparrow} + b_{i,\downarrow}^\dagger \, b_{i,\uparrow} \, b_{i,\uparrow}^\dagger \, b_{i,\downarrow} \right) + \frac{1}{4} \left( b_{i,\uparrow}^\dagger \, b_{i,\uparrow} - b_{i,\downarrow}^\dagger \, b_{i,\downarrow} \right)^2 = \\
&= \frac{1}{2} \left( b_{i,\uparrow}^\dagger \, b_{i,\uparrow} + b_{i,\downarrow}^\dagger \, b_{i,\downarrow} \right) \left( 1 + \frac{1}{2} \left( b_{i,\uparrow}^\dagger \, b_{i,\uparrow} + b_{i,\downarrow}^\dagger \, b_{i,\downarrow} \right) \right), \tag{D.3}
\end{aligned}
$$

where $S^\pm = S^x \pm iS^y$. This requires to constrain the bosons in the following way

$$\sum_\sigma b_{i,\sigma}^\dagger \, b_{i,\sigma} = 2s. \tag{D.4}$$

We can implement this constraint in the functional integral formalism as a $\delta$-function.

$$Z_{spin} = \int \mathcal{D}\{\bar{b}, b\} \, \delta\left(\sum_\sigma b^\dagger \, b - 2s\right) \exp\left\{-\int d\tau \, b^\dagger \, \partial_\tau \, b - \mathcal{H}[b^\dagger, b]\right\}, \qquad (D.5)$$

which can be resolved automatically by transforming into spherical coordinates. To do this we rotate our boson operators by a SU(2) matrix g and find

$$Z_{spin} = \int \mathcal{D}\{\bar{\tilde{b}}, \tilde{b}\} \exp\left\{-\int d\tau \, \tilde{b}^\dagger g^{-1} \partial_\tau g \tilde{b} - \mathcal{H}[\tilde{b}^\dagger, \tilde{b}]\right\}, \qquad (D.6)$$

where $b = \sqrt{2s}g(\tau)\tilde{b}$. The whole $\tau$ dependence is in $g$, therefore the $\tilde{b}^\dagger \partial_\tau \tilde{b}$ term is absent. A parameterization of g can be given by Eq. (E.6). One can easily show that this trivially fulfills our constraint on the Schwinger bosons by simple insertion $b^\dagger b = 2s \, \tilde{b}^\dagger \, g^{-1}g\tilde{b} = 2s$, if we choose $\tilde{b} = \begin{pmatrix} 1 \\ 0 \end{pmatrix}$ in some basis. Using Eq. (E.5) we can express the rotation of the derivatives through a unit vector $\mathbf{n}$. We get

$$Z_{spin} = \int \mathrm{D}\{\bar{b}, b\} \exp\left\{-\int d\tau \, \tilde{b}^\dagger i\boldsymbol{\sigma} \cdot [\mathbf{n} \times \partial_\tau \mathbf{n}] \, \tilde{b} - \mathcal{H}[\tilde{b}^\dagger, \tilde{b}]\right\}. \qquad (D.7)$$

We reinsert the Schwinger boson parameterization and find

$$Z_{spin} = \int \mathrm{D}\{\bar{b}, b\} \exp\left\{-\int d\tau \, 2i\boldsymbol{S} \cdot [\mathbf{n} \times \partial_\tau \mathbf{n}]\right\} \qquad (D.8)$$

where we set $\mathcal{H}[\tilde{b}^\dagger, \tilde{b}] = 0$ for our further analysis. We choose $\mathbf{S} \parallel \mathbf{e}_3$ and note that the cross product stays invariant under a rotation $\mathbf{R}(a \times b) = \mathbf{R}a \times \mathbf{R}b$, the action, however, is only invariant if $\mathbf{SR}^{-1} = \mathbf{S}$. This means, that the rotation is of O(2) type in the $\{1, 2, 3\}$ space:

$$\mathbf{R} = \begin{pmatrix} \mathbf{R}_{O(2)} & 0 \\ 0 & 1 \end{pmatrix}. \qquad (D.9)$$

We use this and explicitly parameterize $\mathbf{n} = \frac{1}{\sqrt{2}}(\mathbf{e}_1 + \mathbf{e}_2)$. If we compute the cross product with explicit insertion of the basis Eqs. (2.7)–(2.9) we find

$$\mathcal{L}_{WZ} = \frac{is\rho_s}{\xi_0} \mathbf{e}_3 \cdot [(\mathbf{e}_1 + \mathbf{e}_2) \times (\partial_\tau \mathbf{e}_1 + \partial_\tau \mathbf{e}_2)] = \frac{2is\rho_s}{\xi_0} \cos(\theta) \, \partial_\tau \psi, \qquad (D.10)$$

where we took the dense impurity limit meaning $\sum\limits_{impurities} \mathcal{L}_{WZ} \to \int \mathrm{dx} \frac{\rho_s}{\xi_0} \mathcal{L}_{WZ}$. This gives the same Wess Zumino action as found in [1, 4]. If we are interested in the Wess Zumino action for the choice of variables we made in Eq. (2.6)

$$\frac{\mathbf{S}_j}{s} = \mathbf{m} + [\mathbf{e}_1 \cos(2k_F x + \alpha) + \mathbf{e}_2 \sin(2k_F x + \alpha)] \sqrt{1 - \mathbf{m}^2}, \qquad (D.11)$$

we can again exploit the O(2) rotational symmetry, this time in the $\mathbf{e}_1'$-$\mathbf{e}_2'$- plane of a orthonormal coordinate system $\{\mathbf{e}_1', \mathbf{e}_2', \frac{\mathbf{S}}{s}\}$. We choose again $\mathbf{m} = \sin\left(\alpha_\parallel\right)\mathbf{e}_3$ and find

$$\mathbf{e}_1' = \cos\left(\alpha_\parallel\right)\mathbf{e}_3 - \left[\mathbf{e}_1\cos\left(2k_Fx + \alpha\right) + \mathbf{e}_2\sin\left(2k_Fx + \alpha\right)\right]\sin\left(\alpha_\parallel\right), \qquad \text{(D.12)}$$

$$\mathbf{e}_2' = \mathbf{e}_1\sin\left(2k_Fx + \alpha\right) - \mathbf{e}_2\cos\left(2k_Fx + \alpha\right), \qquad \text{(D.13)}$$

$$\frac{\mathbf{S}_j}{s} = \sin\left(\alpha_\parallel\right)\mathbf{e}_3 + \left[\mathbf{e}_1\cos\left(2k_Fx + \alpha\right) + \mathbf{e}_2\sin\left(2k_Fx + \alpha\right)\right]\cos\left(\alpha_\parallel\right). \qquad \text{(D.14)}$$

We proceed by parameterizing $\mathbf{n} = \frac{1}{\sqrt{2}}\left(\mathbf{e}_1' + \mathbf{e}_2'\right)$ and find after selecting only non-oscillatory terms in the dense impurity limit

$$\mathcal{L}_{WZ}^{sl} = \frac{2is\rho_s}{\xi_0}\sin\left(\alpha_\parallel\right)\left[\partial_\tau\alpha + \cos\left(\theta\right)\partial_\tau\psi\right], \qquad \text{(D.15)}$$

which again confirms the calculations in [1, 4]. In this calculations we neglected boundary contributions (toplogical terms). The action corresponding to Eq. (D.15) is purely imaginary and the corresponding path integral does not represent a partition function for any classical model. It describes the spin Berry phase of our system, where we separated the dynamics of the fast and the slow modes explicitly. The path integral measure $\{\mathcal{D}\{\Omega_s, \Omega_s'\} = \cos\left(\alpha_\parallel\right)\sin\left(\theta\right)\mathcal{D}\theta\,\mathcal{D}\psi\,\mathcal{D}\alpha_\parallel\,\mathcal{D}\alpha$ now consists of four angles, which does not result in an over counting of d.o.f., since we expect a separation of scales into two fast and two slow variables. Thus there is no double counting of modes, which justifies this approach.

# E

## Appendix E

## Useful relations

In some calculations it is convenient to express a basis of $\mathbb{R}^3$ as $SU(2)$ matrices and vice versa. The following relations might be helpful. We use

$$A = \begin{pmatrix} x \\ y \\ z \end{pmatrix} \rightarrow \begin{pmatrix} z & x-iy \\ x+iy & -z \end{pmatrix} = A^j \sigma_j, \quad A^j = \frac{1}{2}\operatorname{tr}[\sigma_j A], \quad j \in \{x,y,z\}, \quad \text{(E.1)}$$

$$\operatorname{tr}\left[\boldsymbol{\sigma} A^{-1}\sigma_j A\right]\operatorname{tr}\left[\boldsymbol{\sigma} A^{-1}\sigma_{j'} A\right] = 4\delta_{j,j'}, \quad \operatorname{tr}[\boldsymbol{\sigma}\cdots] = \begin{pmatrix} \operatorname{tr}[\sigma_x\cdots] \\ \operatorname{tr}[\sigma_y\cdots] \\ \operatorname{tr}[\sigma_z\cdots] \end{pmatrix}, \quad \text{(E.2)}$$

and parameterize an orthogonal basis $\{\mathbf{e}_1, \mathbf{e}_2, \mathbf{e}_3\}$ as follows

$$\mathbf{e}_{1,2,3} = \frac{1}{2}\left[\boldsymbol{\sigma} g\sigma_{x,y,z} g^{-1}\right], \quad \mathbf{e}_3 = [\mathbf{e}_1 \times \mathbf{e}_2]. \quad \text{(E.3)}$$

We can rewrite a scalar product involving $\boldsymbol{\sigma}$ as follows

$$\boldsymbol{\sigma} \cdot \mathbf{e}_{1,2,3} = \frac{1}{2}g\sigma_{x,y,z}g^{-1} \quad \rightarrow \quad \boldsymbol{\sigma} \cdot [\mathbf{e}_1 \pm i\,\mathbf{e}_2] = g\sigma_\pm g^{-1}, \quad \sigma_\pm = \frac{\sigma_x \pm i\sigma_y}{2}, \quad \text{(E.4)}$$

or do the inverse and express the SU(2) matrices via a unit vector

$$g = i\boldsymbol{\sigma} \cdot \mathbf{n}, \quad |\mathbf{n}| = 1 \quad \rightarrow \quad g^{-1}\partial_a g = i\boldsymbol{\sigma} \cdot [\mathbf{n} \times \partial_a \mathbf{n}]. \quad \text{(E.5)}$$

One explicit parameterization of g can be given by

$$g = \begin{pmatrix} e^{i\frac{\psi+\phi}{2}}\cos\left(\frac{\theta}{2}\right) & -e^{i\frac{\phi-\psi}{2}}\sin\left(\frac{\theta}{2}\right) \\ e^{-i\frac{\phi-\psi}{2}}\sin\left(\frac{\theta}{2}\right) & e^{-i\frac{\psi+\phi}{2}}\cos\left(\frac{\theta}{2}\right) \end{pmatrix} \quad \text{(E.6)}$$

Erklärung:

Hiermit erkläre ich, die vorliegende Arbeit selbständig verfasst zu haben und keine anderen als die in der Arbeit angegebenen Quellen und Hilfsmittel benutzt zu haben.

München, der 8. November 2019

Florian Stäbler